The effect of temperature, water vapor and thermal activation on Pt/TiO_2/Ti electromotive force cells

Inaugural-Dissertation

zur Erlangung des Doktorgrades der

Mathematisch-Naturwissenschaftlichen Fakultät

der Heinrich-Heine-Universität Düsseldorf

vorgelegt von

Ömer Cakabay

aus Bingöl (Türkei)

Düsseldorf, Juni 2016

Aus dem Institut für Experimentelle Physik der kondensierten Materie

der Heinrich-Heine-Universität Düsseldorf

Gedruckt mit der Genehmigung der Mathematisch-Naturwissenschaftlichen Fakultät der Heinrich-Heine-Universität Düsseldorf

Referent: Prof. Dr. K. D. Schierbaum

Korreferent: Prof. Dr. Mathias Getzlaff

Tag der mündlichen Prüfung: 06. Oktober 2016

For Yıldırım

"(…)

It matters not how strait the gate,

How charged with punishments the scroll,

I am the master of my fate:

I am the captain of my soul."

William Ernest Henley

The work described in this thesis consists of three **peer-reviewed papers**, which constitute the following chapters:

- Chapter 1: Cakabay, Ö.; El Achhab, M.; Schierbaum, K. Thermal properties of solid-state $Pt/TiO_2/Ti$ emf cells studied by microcalorimetry. *Appl. Phys. A* 2015, *118*, 1127-1132.

- Chapter 2: Cakabay, Ö.; El Achhab, M.; Schierbaum, K. Effect of water vapor on $Pt/TiO_2/Ti$ electromotive force cells. *J. Phys. Chem. C* 2016, DOI: 10.1021/acs.jpcc.6b01315.

- Chapter 3: Cakabay, Ö.; Schierbaum, K. Thermal activation of $Pt/TiO_2/Ti$ emf cells. Submitted, 2016.

Moreover, the author of this thesis is involved in the **following invention** and **publications**, which are part of this thesis:

Patent

- Vorrichtung zur Erzeugung einer elektromotorischen Kraft und Verfahren zum Herstellen solchen, DE 10 2013 102 485.8, Applicant: Heinrich-Heine-Universität Düsseldorf.

Poster

- Cakabay, Ö.; El Achhab, M.; Schierbaum, K. Auf $Pt/peO\text{-}TiO_2/Ti$ basierender EMK-Generator, *DPG, Regensburg, 2013.*

- Cakabay, Ö.; El Achhab, M.; Schierbaum, K. Microcalorimetric study of the hydrogen-to-water oxidation on solid-state $Pt/TiO_2/Ti$ emf cells, *DPG, Dresden, 2014.*

The author of this thesis is also involved in the following **invention** and **publication**, which are not contained in this thesis:

Patent

- Sensoranordnung und Verfahren zum Herstellen einer Sensoranordnung, DE 10 2012 108 997.3, Applicant: Heinrich-Heine-Universität Düsseldorf.

Poster

- El Achhab, M.; Cakabay, Ö.; Schierbaum, K. Gassensoren mit Titanoxidschichten, *12.Dresdner-Sensor Symposium, Dresden, 2016.*

Summary

In this thesis, the effects of temperature, water vapor, and thermal activity on $Pt/TiO_2/Ti$ electromotive force (emf) cells are studied. The obtained results were presented in three separate chapters. Titanium dioxide layers were produced via a plasma electrolytic oxidation process and Pt coating was applied using a pasting process. The experiments were performed in a programmable gas flow system consisting of two pressurized gas bottles (one with 3.5 vol % H_2 in synthetic air, the other with synthetic air only), mass flow controllers for adjusting the overall gas flow and the concentration of H_2, two measurement chambers (one for the microcalorimetric measurements and the other for measuring the generated current) and a gas washing bottle for adjusting the relative humidity (RH) of the air.

In the first chapter, we investigated the effect of temperature on $Pt/TiO_2/Ti$ emf cells. We found that generated current exhibits significant temperature dependence. At room temperature these structures exhibit steady-state and high value current densities of up to 25 mA/cm^2 during exposure to H_2/air mixtures. However, when the temperature is increased, the current decreases, and at temperatures of $T > 50$ °C it breaks down completely.

In order to explain the effect of temperature on the generated current, we used an isothermal-operated microcalorimeter setup. It consists of a Pt100 resistor and a microheater attached to the $Pt/TiO_2/Ti$ sample. The microcalorimeter setup was utilized to determine the heat of reaction released during H_2 oxidation at different temperatures. Electrical power was dissipated within the microcalorimeter to increase the temperature of the $Pt/TiO_2/Ti$ sample. Upon exposure to the adjusted hydrogen-oxygen mixtures, the electrical power was observed to decrease to a certain value depending on the *T*. The obtained difference between the values of electrical power was then used to identify the rates of H_2-to-H_2O turnover. Three different regions (kinetic region, pore diffusion and film diffusion) result from plotting the logarithm of experimental determined values of H_2O against the

reciprocal values of adjusted temperature (Arrhenius diagram). This reveals a significant temperature dependence of reaction rate of H_2O which correlates well with the temperature dependence of the generated current. On the basis of these findings, we postulate that that i) the diffusion of H_2 and O_2 molecules in the porous Pt coating at around room temperature (kinetic region) is fast enough to allow a sufficient amount of reactants to penetrate to the TiO_2 and generate constant and high densities of generated current; ii) at $T > 50$ °C, however, the pore diffusion becomes rate-determining. This implies that the rate of hydrogen oxidation in the region of pore diffusion is relatively high and therefore, one may assume that the reactants convert in the pores of the platinum catalyst before reaching the TiO_2. This is in correspondence with the breakdown of generated current at 65 °C.

In the second chapter, the effect of water vapor on the generated current was investigated using microcalorimetry, current-voltage (*I-V*) characteristics and electrochemical impedance spectroscopy. The results from the *I-V* characteristics confirm that water vapor has a significant effect on generated current. It was found that adding water vapor to the hydrogen-to air mixture leads to a volcano-type behavior of short-circuit current density J_{sc}, with a maximum effect at 10 % RH, and that J_{sc} drops markedly at RH above 20 %. Interestingly, the open-circuit voltage V_{oc} always increases with increasing humidity.

In this chapter, as in the first one, the microcalorimetric measurements were carried out, in order to determine the rates of catalytic turnover of H_2 to H_2O at $Pt/TiO_2/Ti$ samples. In this measurement, however, the temperature of $Pt/TiO_2/Ti$ samples was maintained constant at 20 °C, and RH was increased successively from 0% to 40%. It was observed that the turnover of H_2 to H_2O decreases with increasing RH and reveals no similar volcano-type behavior. This result indicates that in the presence of water vapor, the TiO_2-related surface reactions play a predominant role in the reduction of efm generation.

Electrochemical impedance spectroscopy was used to determine the charge transport and relaxation properties of Pt/TiO_2/Ti layer structures in both humid air and humid air containing hydrogen. In both cases, two semicircles were observed in the resulting Nyquist plot (a representation of the real and imaginary parts of impedance). However, they show markedly different transients depending on the presence of hydrogen. Both semicircles representing typically (*RC*) equivalent circuit diagrams were attributed to the electrical properties of the grain boundaries of TiO_2 and the electrode polarization effect. Correspondingly, both resistances represent the resistance (R_{gb}) of the grain boundaries of TiO_2 and charge transfer resistance (R_{ct}) at the interface of Pt/TiO_2, respectively. Upon adding RH to the hydrogen-in-air mixture, the reciprocal of the sum of both resistances $(R_{gb} + R_{ct})^{-1}$ was found to exhibit similar volcano-type behavior as J_{sc}. Furthermore, the sum of both resistances ($R_{gb} + R_{ct}$) was observed to correlate well with the internal resistance (V_{oc}/I_{sc}) of Pt/TiO_2/Ti emf cells calculated from the *I-V* curves.

It was suggested that the electromotive force is arises from the difference in the hydrogen partial pressures at the Pt/TiO_2 interface and on the distant TiO_2 surface sites, under the condition that the partial pressure of hydrogen at Pt/TiO_2 interface is smaller than the partial pressure of TiO_2 due to the large catalytic activity of Pt. We further suggest that the interaction of hydrogen with the TiO_2 surface results in the formation of two hydroxyls groups at oxygen bridging sites. This reaction releases two electrons per H_2 molecule to the TiO_2 due to electrostatic neutrality. The electron transport was assumed to occur via an electron hopping process over Ti^{+4} lattice ions to titanium contact.

The results of *I-V* characteristics recorded in the humid air in the absence of hydrogen indicate that the adsorption of H_2O molecules reduces the oxygen acceptor states in the interface of the Pt/TiO_2. This can be regarded as a “quasi-donor” effect of water. However, a reverse behavior (acceptor-type effect) has been found for H_2O adsorption in the presence of H_2. The effect was interpreted

as a blocking effect of the oxygen bridging sites on the TiO_2 surface at which the hydrogen adsorption and the resulting release of electrons to TiO_2 take place.

The observed maximum current densities at 10% RH was related to the enhancement of electron transport by wet electron states, whereas the increase in the open-circuit voltage was attributed to the voltage drop in the double layer at the Pt/TiO_2 interface that increases with increasing RH.

In the last chapter, the effect of thermal activation on aged $Pt/TiO_2/Ti$ emf cells was examined. It was observed that aging significantly affects the generated current density of $Pt/TiO_2/Ti$ emf cells. The aged samples stored in air were heat-treated by a short thermal process known as “flashing”. In order to determine the differences before and after flashing, the aged and flashed TiO_2 samples were characterized using scanning electron microscopy (SEM), atomic force microscopy (AFM), Raman microscopy and X-ray photoelectron spectroscopy (XPS). The images resulting from SEM and AFM show similar porous microstructures before and after flashing. The analysis of Raman spectroscopy shows that the TiO_2 structure consists of a rutile and anatase mixture with a predominant rutile phase which remains unchanged after flashing. Also, no visible changes were found in the XPS spectra after flashing, indicating that no Ti-suboxides were formed during the flashing process.

The characterization of the aged and flashed $Pt/TiO_2/Ti$ samples was further enhanced using electrochemical impedance spectroscopy (EIS) in the flow apparatus in both the absence and presence of hydrogen. The results of EIS were consistent with the behavior of the generated current before and after flashing. After flashing, the resistance of the grain boundaries of TiO_2 (R_{gb}) and the charge transfer resistance (R_{ct}) at the interface of the Pt/TiO_2 were found to decrease by three orders of magnitude and six orders of magnitude, respectively.

A high concentration of oxygen-induced interface states was assumed to be a reason for the aging behavior of the $Pt/TiO_2/Ti$ samples. These can lead to a space

charge layer at the grain boundaries of TiO_2 crystallites and accordingly to an energy barrier for electron transport between adjacent TiO_2 crystallites. The flashing could reactivate the aged samples by removing a large amount of the adsorbed oxygen at the surface and grain boundaries.

Zusammenfassung

In Rahmen der vorliegenden Dissertation wurde der Effekt von Temperatur, Wasserdampf und thermischer Aktivierung auf die elektromotorische Kraft (EMK)-Generation der $Pt/TiO_2/Ti$-Zellen untersucht. Die erhaltenen Ergebnisse wurden separat in drei Kapiteln dargestellt. Titandioxid-Schichten wurden durch plasmaelektrolytische Oxidation und Platin-Beschichtung unter Verwendung eines Paste-Verfahrens hergestellt. Die Experimente wurden in einem programmierbaren Gasströmungssystem durchgeführt, bestehend aus zwei Druckgasflaschen (3.5 Vol % H_2 in synthetischer Luft und nur synthetische Luft), drei Massenflussregler zur Einstellung des Gesamtgasflusses und der Konzentration von H_2, zwei Messkammern (eine für die Mikrokalorimetrie-Messungen und eine andere für die Messungen des generierten Stroms) und eine Gaswaschflasche für das Einstellen bestimmter relativer Luftfeuchten.

Im ersten Kapitel wurde der Einfluss der Temperatur auf die EMK-Generation der $Pt/TiO_2/Ti$-Proben untersucht. Gefunden wurde, dass der generierte Strom eine drastische Temperaturabhängigkeit aufweist. Bei etwa Raumtemperatur zeigen diese Strukturen konstante und hohe Werte der Stromdichten bis zu 25 mA/cm^2 bei der Exposition mit H_2/Luft-Gemische. Mit steigender Temperatur nimmt der Strom jedoch ab, und er bricht sogar bei Temperaturen $T > 50$ °C komplett zusammen.

Um den Effekt der Temperatur auf den generierten Strom zu erklären, haben wir ein isotherm betriebenes Mikrokalorimeter aufgebaut, mit welchem die freigesetzte Reaktionswärme während der H_2-Oxidation bei unterschiedlichen Temperaturen bestimmt wurde. Zur Konstanthaltung der eingestellten Probentemperatur wurde dem Mikrokalorimeter eine elektrische Leistung zugeführt. Es wurde beobachtet, dass die Leistung am Mikrokalorimeter nach H_2-Zugabe als Ergebnis der exothermen Reaktion abnimmt. Der Unterschied zwischen den konstanten Werten der Leistung wurde zur Bestimmung des Umsatzes der H_2-zu-H_2O-Oxidation verwendet. Aus der Auftragung des

Logarithmus der experimentell bestimmten H_2O-Werte gegen die reziproken eingestellten Werte der Temperatur (Arrhenius-Diagramm) haben sich drei verschiedene Bereiche (kinetischer Bereich, Porendiffusions- und Filmdiffusionsbereich) ergeben. Arrhenius-Diagramm offenbart eine deutliche Temperaturabhängigkeit der H_2O-Reaktionsgeschwindigkeit, die mit der Temperaturabhängigkeit des generierten Stroms gut korreliert. Auf der Grundlage dieser Erkenntnisse postulieren wir, dass i) bei etwa Raumtemperatur (kinetische Region) die Diffusion von H_2 und O_2-Moleküle in den Poren des Platinkatalysators schnell genug ist, so dass eine ausreichende Menge des Reaktionspartner an das TiO_2 gelangen und daher zur konstanten und großen Werten des generierten Stroms führen kann, und dass ii) bei $T > 50$ °C die Porendiffusion geschwindigkeitsbestimmend wird. Im letzteren bedeutet dies, dass die katalytische Oxidation vom Wasserstoff im Bereich der Porendiffusion schnell abläuft. Daher können die Reaktionspartner bereits in den Poren des Platinkatalysators umgewandelt werden, ohne dass sie an das Titanoxid gelangen. Dies steht in Übereinstimmung mit dem Zusammenbruch des generierten Stroms bei 65 °C.

Im zweiten Kapitel wurde der Effekt der Feuchtigkeit auf den geneierten Strom mit Hilfe der Mikrokalorimetrie, der Strom-Spannung (*I*-*V*)-Kennlinie und der elektrochemischen Impedanzspektroskopie untersucht. Die Ergebnisse von *I*-*V*-Kennlinien bestätigen einen signifikanten Effekt der Feuchtigkeit auf den generierten Strom. Wir beobachten, dass der steigende Wasserdampf, der dem Wasserstoff-Luft-Gemisch zugegeben wird, ein vulkanartiges Verhalten der Kurzschlussstromdichte (J_{sc}) mit einem Maximum bei 10% relativer Feuchtigkeit (RH) verursacht; eine deutlich starke Abnahme von J_{sc} wurde insbesondere bei RH > 20% beobachtet. Interessanterweise hat die Leerlaufspannung V_{oc} mit steigender Feuchtigkeit ständig zugenommen.

Des Weiteren wurden mikrokalorimetrische Messungen unternommen, um den katalytischen Umsatz von H_2-zu-H_2O auf der $Pt/TiO_2/Ti$-Schichtstruktur zu

bestimmen. Während dieser Messungen wurde die Probentemperatur bei 20 °C konstant gehalten und RH von 0% bis 40 % sukzessiv erhöht. Beobachtet wurde, dass die Umsatzrate von H_2-zu-H_2O bei Zugabe von RH ständig abnimmt, welche jedoch kein ähnliches vulkanartiges Verhalten zeigt. Dieses Ergebnis deutet darauf hin, dass in Anwesenheit vom Wasserdampf TiO_2-oberflächenbezogene Reaktionen eine vorherrschende Rolle in der Verringerung der EMK-Generation spielen.

Die elektrochemische Impedanzspektroskopie wurde verwendet, um den Ladungstransport und die Relaxationseigenschaften von Pt/TiO_2/Ti-Schichtstrukturen in feuchter Luft und in feuchter Luft mit Wasserstoff zu bestimmen. In beiden Fällen wurden zwei Halbkreise in dem Nyquist-Diagramm (Darstellung der realen und imaginären Teile der Impedanz) beobachtet. Allerdings zeigen sie deutlich unterschiedliche Transienten. Die beiden Halbkreise (jeder stellt typischerweise ein RC-Ersatzschaltbild dar) wurden den elektrischen Eigenschaften der Korngrenzen von TiO_2 und dem Elektrodenpolarisationseffekt zugeschrieben. Entsprechend präsentieren die beiden Widerstände in der Ersatzschaltung den Widerstand der Korngrenzen von TiO_2 (R_{gb}) und den Charge-Transfer-Widerstand (R_{ct}) in der Grenzfläche von Pt/TiO_2. Wir finden, dass der Kehrwert der Summe der beiden Widerstände $(R_{\mathrm{gb}} + R_{\mathrm{ct}})^{-1}$ bei der Zugabe von RH zum Wasserstoff-in-Luft-Gemisch ein ähnliches vulkanartiges Verhalten wie J_{sc} aufweist. Außerdem zeigt der Innenwiderstand ($V_{\mathrm{oc}}/I_{\mathrm{sc}}$) von Pt/$TiO_2$/Ti-Zelle, welcher sich aus *I-V*-Kennlinien berechnen lässt, eine gute Korrelation mit der Summe von den beiden Widerständen ($R_{\mathrm{gb}} + R_{\mathrm{ct}}$).

Es wird vorgeschlagen, dass die elektromotorische Kraft durch einen Unterschied zwischen den Wasserstoff-Partialdrücken auf der Pt/TiO_2-Grenzfläche und auf den fernen TiO_2-Oberflächenstellen erzeugt wird. Dabei ist es zu erwarten, dass der Partialdruck von Wasserstoff an Pt/TiO_2-Grenzfläche aufgrund der großen katalytischen Aktivität von Pt kleiner als der Partialdruck auf TiO_2 ist. Wir haben

ferner vorgeschlagen, dass die Wechselwirkung vom Wasserstoff mit der TiO_2-Oberfläche zur Bildung von zwei Hydroxylgruppen (OH-Gruppen) auf den Sauerstoff-Brückenstellen führt. Wegen der elektrostatischen Neutralität setzt diese Reaktion zwei Elektronen per H_2O-Molekül in das Leitungsband des Titandioxids frei. In Anlehnung an die starke Elektron-Phonon-Kopplung im TiO_2 wurde angenommen, dass der Elektronentransport in Titandioxid durch Elektron-Hopping-Prozess über Ti^{4+} Gitterionen stattfindet.

Die Ergebnisse von *I-V*-Kennlinien, die in feuchter Luft in Abwesenheit vom Wasserstoff aufgenommen wurden, deuten darauf hin, dass die Adsorption von H_2O-Molekülen die Sauerstoff-Akzeptorzustände in der Grenzfläche von Pt/TiO_2 reduziert. Dies wurde als einen "quasi-Donator"-Effekt vom Wasser betrachtet. Aus den Ergebnissen der *I-V*-Kennlinien, die in feuchter Luft in Anwesenheit Wasserstoff aufgenommen wurden, geht jedoch ein umgekehrtes Verhalten (Akzeptor-Typ Effekt) vom Wasser hervor. Dieser Effekt wurde interpretiert als einen blockierenden Effekt von Sauerstoff-Brückenstellen auf der TiO_2-Oberfläche, worauf die Adsorption vom Wasserstoff und die dadurch verursachte Freisetzung der Elektronen stattfinden.

Die beobachtete maximale Stromdichte bei 10 % RH wurde mit der Verbesserung des Elektronentransports durch "wet"-Elektronenzustände in Verbindung gebracht, während die Erhöhung der Leerlaufspannung dem Spannungsabfall in der Doppelschicht in der Pt/TiO_2-Grenzfläche zugeschrieben wurde.

Im letzten Kapitel wurde die thermische Aktivierung von gealterten $Pt/TiO_2/Ti$-Proben untersucht. Festgestellt wurde, dass die Alterungserscheinungen die generierten Stromdichten von $Pt/TiO_2/Ti$-Proben signifikant beeinträchtigen. Die gealterten Proben, die an der Luft gelagert wurden, wurden durch einen kurzen thermischen Prozess (sog. Flashen) behandelt. Um die Unterschiede vor und nach Flashen zu bestimmen, wurden die gealterten und geflashten TiO_2-Proben durch Rasterelektronenmikroskopie (REM), Rasterkraftmikroskopie (AFM), Raman-Mikroskopie und Röntgenphotoelektronenspektroskopie (XPS) charakterisiert.

Die REM- und AFM-Aufnahmen vor und nach Flashen zeigen ähnlich poröse Mikrostrukturen mit verschieden Vertiefungen. Die Ramanspektroskopische Untersuchung zeigt, dass TiO_2-Struktur aus Rutil und Anatas mit einem prädominierten Rutil-Phasenanteil besteht. Das Rutil/Anatas-Verhältnis bleibt nach Flashen unverändert. Auch bei XPS-Spektren wurden keine sichtbaren Änderungen nach Flashen gefunden, welches darauf hindeutet, dass keine Ti-Suboxide während des Flashen-Vorgangs gebildet wurden.

Die weitere Charakterisierung der gealterten und geflashten Pt/TiO_2/Ti-Proben erfolgte mit der elektrochemischen Impedanzspektroskopie (EIS) in der Strömungsapparatur in Ab- und Anwesenheit vom Wasserstoff. Die Ergebnisse von EIS sind konsistent mit dem Verlauf des generierten Stroms vor und nach Flashen. Es wurde gefunden, dass der Flashen den Innenwiderstand von Pt/TiO_2/Ti-Zelle, bestehend aus dem Widerstand der Korngrenzen von TiO_2 (R_{gb}) und den Charge-Transfer-Widerstand (R_{ct}) in der Grenzfläche von Pt/TiO_2, bis zur drei Größenordnungen verringert hat. R_{gb} hat sich sogar um etwa sechs Größenordnungen verringert.

Für die Alterung der Proben wurde als Ursache eine hohe Konzentration von Sauerstoff-induzierten Grenzflächenzuständen angenommen. Diese führen zu einer Raumladungsschicht an den Korngrenzen von TiO_2-Kristalliten und dementsprechend zu einer Energiebarriere für den Elektronentransport zwischen den benachbarten TiO_2-Kristalliten. Der Flashen der gealterten Proben führt zu ihren anfänglichen aktiven Zuständen, indem er eine große Zahl des adsorbierten Sauerstoffs entfernt.

Contents

Introduction

Ever-increasing industrialization and a large and growing population pose the pivotal question of how best to satisfy the world's increasing future energy needs. A vast majority of countries actively seek out sustainable solutions to their energy needs. In almost all energy scenarios, hydrogen as an energy carrier emerges to be an important candidate. The major reason is that the heat (or enthalpy) of the reaction $H_2 + 1/2\,O_2 \rightarrow H_2O(g)$ at standard conditions (289.15 K and 1 atm) equals -241.98 kJ/mol, a large portion of which (-228.74 kJ/mol, free reaction enthalpy) [1] can be converted into electrical work. Fuel cells are probably the most prominent example that comes to mind when thinking about devices in which hydrogen is directly used to produce electrical energy. Figure 1 illustrates the principles of a traditional double-chamber fuel cell.

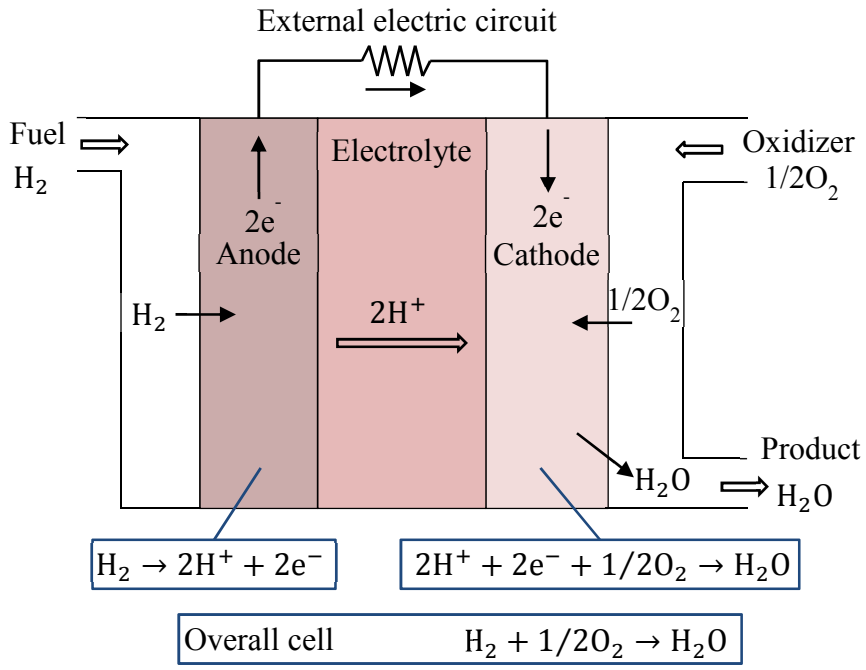

Figure 1. Schematic diagram of a hydrogen/oxygen fuel cell.

Although various types of fuel cells with many different architectures and configurations are currently under development and investigation, they can mainly be categorized into two types: single- and double-chamber fuel cells. The single-

chamber fuel cells offer a simpler design than double-chamber fuel cells: Both electrodes are located in one compartment, into which the fuel-oxidant-mixture is directly supplied [2]. However, due to catalytic activity and ion conduction, both the electrodes and the electrolyte materials used in the single-chamber fuel cells can only operate at high temperatures. Furthermore, highly selective anode and cathode materials are necessary for the fuel oxidation and oxygen reduction processes, respectively [3].

A room-temperature solid-state $Pt/TiO_2/Ti$ device formed by platinum coating and plasma electrochemically oxidized titanium foils was reported to generate current densities of up to 20 mA/cm^2 and an electromotive force of up to 465 mV during the hydrogen-to-water-oxidation [4]. The catalytic oxidation of carbon monoxide on thin film Pt/TiO_2 nanodiodes was firstly observed to generate a steady-state current ("chemicurrent") under zero-bias conditions [5].

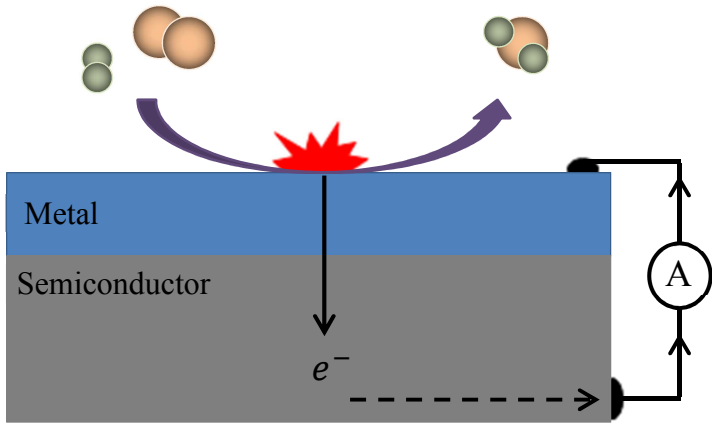

Figure 2. Schematic representation of chemicurrent generation in a nanodiode. The interaction of molecules with the metal surface creates hot electrons. The thickness of the diode's metal layer must be equivalent to the mean free path of the hot electrons so that they can cross the film and reach the metal-semiconductor interface. Hot electrons having kinetic energies higher than the Schottky barrier can then surmount the barrier and move into the semiconductor, where they can be measured as chemicurrent.

The chemicurrent has been related to the exothermic chemical reactions on the catalytic metal surface [6-10]; transfer of the resulting heat of reaction to the

metal creates the distribution of energetic electrons referred to as “hot electrons” in the metal. These hot electrons can be ballistically injected over the Schottky barrier into the space charge region of the semiconductor, where they are detected as a chemicurrent in the device. The principle of the detection of the chemicurrent is shown in Figure 2. The hot electron effect requires thin metal layers with thicknesses on the order of the mean free path of the hot electrons (5-10 nm) [5], that is, however, not necessary for the solid-state Pt/TiO_2/Ti electromotive force (emf) cells. The observed current yield of such thin film Pt/TiO_2 catalytic nanodiodes is very low compared to the Pt/TiO_2/Ti emf cells. Therefore, it is difficult to establish a consistency between the hot electron model and the generation of electromotive force in the Pt/TiO_2/Ti devices.

Schierbaum et al.[10] explained the generated current and the related electromotive force of Pt/TiO_2/Ti cells using a model based on an analogy regarding the effects in galvanostatic solid electrolyte sensors [11]. The model suggests that the emf generation is caused by a chemical potential gradient of hydrogen resulting from different hydrogen partial pressures in the porous Pt/TiO_2/Ti structure. In this model, the structure was divided into two compartments as shown in Figure 3. Compartment I represents the partial pressure of hydrogen in porous TiO_2 close to Pt contact, while Compartment II shows the partial pressure of hydrogen at the Pt surface which is expected to be lower than in Compartment I due to the large catalytic activity of Pt.

The adsorption of hydrogen on TiO_2 (110) surfaces has been previously investigated by Kunat et al. [12]. The results indicate the formation of an H (1×1) TiO_2 surface during atomic hydrogen exposure. Further experiments on the interaction of TiO_2 (110) with atomic hydrogen reveal the formation of (partially) hydroxylated TiO_2 surfaces [13,14]. It has been recently proposed that the diffusion of hydrogen in TiO_2 in the presence of hydroxyl ions proceeds by proton jumps from one O^{2-} ion to another [15]. Furthermore, it is well-known that metal

oxides are reduced by the hydrogen that forms the oxygen vacancies at surface sites.

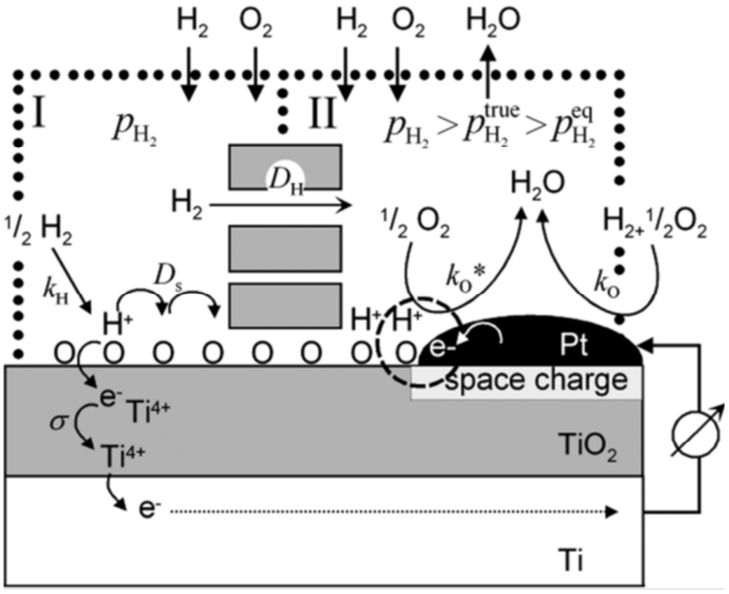

Figure 3. Schematic representation of emf generation in a Pt/TiO_2/Ti structure [10].O denotes the oxygen atoms on the TiO_2 surface, which together with hydrogen form hydroxyl groups on the TiO_2 surface. The dashed circle marks the three-phase boundary (gas/Pt/TiO_2) at which the hydrogen oxidation takes place. The rate constants of the hydroxylation, the water formation at the three-phase boundary and the water formation on platinum are denoted by k_H, k_0^*, and k_0, respectively. P_{H_2} represents the partial pressure of hydrogen in porous TiO_2 close to Pt contact, while the $P_{H_2}^{true}$ and $P_{H_2}^{eq}$ are the true and equilibrium values of partial pressure of hydrogen at the Pt surface.

According to the aforementioned model of emf generation, the interaction of hydrogen with TiO_2 film leads to the formation of charged surface hydroxyl groups at O-bridging surface sites. The reaction then releases two electrons per hydrogen molecule into the TiO_2 which are transported via an electron hopping process over Ti^{4+} ions to the titanium contact as shown in Figure 3. At three-phase boundary (gas/Pt/TiO_2), marked with dashed circle in Figure 3, these electrons and the hydrogen protons diffused out from the TiO_2 film to the Pt contact react with the oxygen to water, while at Pt surface, a direct catalytic oxidation of hydrogen takes place.

This thesis deals with the effect of temperature, water vapor and thermal activation (flashing) on Pt/TiO_2/Ti electromotive force (emf) cells. The Pt layers were prepared using a pasting method, while the porous TiO_2 films, which play a key role in the generation of the large current densities in Pt/TiO_2/Ti emf cells, were formed by plasma electrolytic oxidation (PEO). The process of PEO [16] is similar to the electrochemical process of anodic oxidation that is performed at higher voltages resulting in the mechanically stable and well-adhered porous oxide coatings for metals such as titanium [17] and aluminum [18]. This process is also known as micro-arc oxidation (MAO) [19] or anodic spark discharges (ASD) [20].

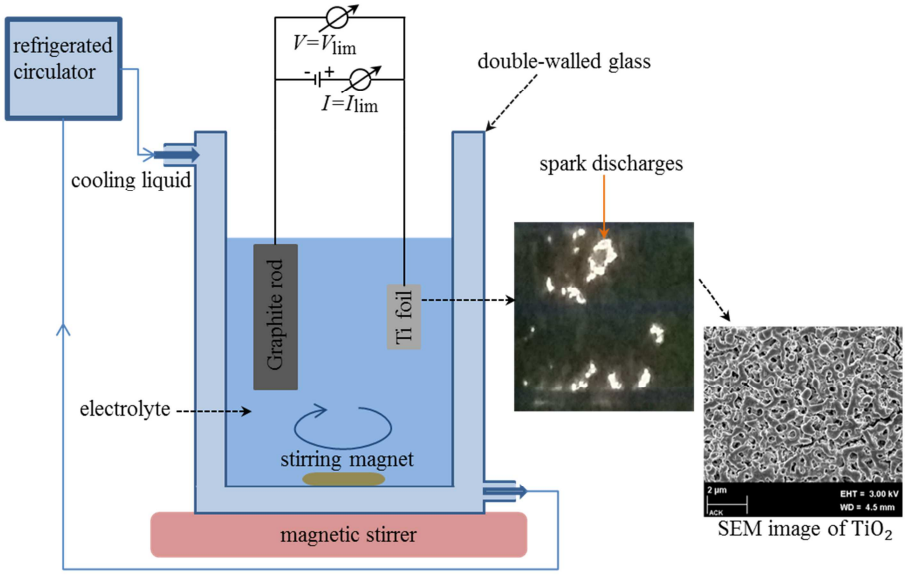

Figure 4. Schematic representation of the electrolyte chamber. The plasma electrolytic oxidation of Ti foils is made in a water-jacketed double-walled glass container filled with a 14M sulfuric acid electrolyte. A graphite rod is used as cathode. Spark discharges occurring during the oxidation lead to an increase in the temperature of the electrolyte in the chamber. Therefore, a refrigerated circulator (FP50, Julabo) is connected with the tempering glass. This helps keep the temperature constant during oxidation. The insets show the occurrence of spark discharges on the surface of growing oxide and an SEM image of a TiO_2 sample, respectively.

The most obvious observation during the PEO process is the occurrence of micro-discharges when the voltage applied is above the breakdown voltages of growing

oxides. The created conditions of high temperatures up to 10^4 K and pressures up to 10^3 MPa in the central zone of the discharge channels leading to the plasma thermochemical reactions result in the formation of ceramic-like oxide films [21].

The technique used here to yield the plasma electrochemically oxidized titanium foils is a special preparation method developed by the authors in Ref [22]. The method is based on the combination of potentiostatic and galvanostatic oxidation of titanium foils and requires a strong acidic electrolyte (14M sulfuric acid) under constant stirring, the successive increase in applied voltage and the limitation of current flowing through growing oxides. A schematic representation for the electrochemical preparation technique is shown in Figure 4.

The structural investigation of TiO_2 samples prepared using this technique [22] show a strong dependence of porosity and phase distribution on the anodization voltages; with increasing voltage, pores become much more numerous and much larger, and a thermal transformation of anatase to rutile occurs. A structural model has been proposed to explain the evolution of titanium dioxide's microstructure during oxidation as a function of time and voltage [22]. This model suggests three ranges at which certain etching and oxidation processes may take place; in the first range, successive increases in voltage up to 71 V leads to the formation of a thin primary anatase layer on the titanium foil which grows according to the conventional anodization mechanism. Further successive increases from 71 V to 123 V - the second range - may adjust the conditions of plasma electrolytic oxidation. During this period, short-lived electrical micro-discharges at single sites on the surface are observed. These may result in the dissolution of the primary anatase layer and of the titanium foil, and therefore to the formation of singular pores. After this breakdown, the degraded sites can be healed again by anodic oxidation. At the end of this step of the process, a porous TiO_2 layer consisting of secondary anatase with a small amount of rutile is formed. The rutile exists presumably at the sites which were repeatedly in contact with the spark discharges. During the final step of the process, the anodization voltage is

increased further from 123 V to 157 V. In this third range, strong and dense spark discharges occur. These result in the harsh degradation of the secondary anatase layer and the formation rutile on the oxide surface. At the end of the entire oxidation process, a particular microstructure of the porous oxide layer with a predominant rutile phase is formed. These oxide structures show good thermal, mechanical, and electrical properties which provide the generation of electromotive force in $Pt/TiO_2/Ti$ samples with particularly high current densities.

The aim of the work reviewed here is to determine the optimum operating conditions for the $Pt/TiO_2/Ti$ emf cells by investigating the effects of temperature, water vapor, and thermal activation on these emf cells.

The first condition for constant and high current densities of $Pt/TiO_2/Ti$ emf cells is a continuous and constant supply of hydrogen from the gas phase to the $Pt/TiO_2/Ti$ emf cell, e.g., in a stationary flow condition. Second, a sufficient transport of hydrogen through the porous Pt film to the titanium dioxide sites is required. As mentioned above, the chemical reactions are always accompanied by an energy release. For example, the reaction enthalpy for H_2 oxidation in a fuel cell at room temperature is equal to -284.7 kJ/mol, of which 237.3 kJ/mol is used to produce an electromotive force of 1.23 V and the remaining 47.3 kJ/mol manifests as heat [23]. Thus, it may be expected that the released reaction heat during H_2 oxidation in $Pt/TiO_2/Ti$ emf cells leads to an increase in the catalytic activity of Pt. As a consequence, a large amount of hydrogen might be converted directly to water in the porous Pt coating without reaching the titanium dioxide. Thus, one can assume that the direct catalytic oxidation of hydrogen in platinum competes with chemical reactions generating the current and related electromotive force, leading to a decrease in the efficiency of such cells.

On the other hand, large number of water molecules can also be formed during H_2 oxidation. It is well known that water affects the hydrogen-to-water oxidation over the Pt catalyst [24,25] and that it interacts with the TiO_2 surface [26-30]. During its interaction with TiO_2, a water molecule can either directly dissociate at

oxygen vacancies sites on the TiO_2 surface to form two surface hydroxyl (OH) groups or physically adsorb on these partially hydroxylated surfaces [29,30]. Recent studies on photo-induced electron transfer at the $H_2O/TiO_2(110)$ interface using time-resolved two-photoemission spectroscopy have shown an unoccupied electron state 2.4 eV above the Fermi level. On the basis of the chemisorption properties of H_2O and the density functional theory calculations, this state was attributed to a partially hydrated "wet-electron" state [31,32]. Fischer et al. [33] investigated electron transfer in the wet-electron system using state-of-the-art ab initio nonadiabatic molecular dynamics. They reported a strong coupling between H_2O and TiO_2 surfaces leading to the creation of conditions for the sub-10 fs ultrafast electron transfer via both adiabatic and non-adiabatic electron transfer mechanisms. For the $Pt/TiO_2/Ti$ system, it is still uncertain whether reaction processes, especially the rate of dissociative H_2 adsorption with active sites on TiO_2 surfaces and electron transport through porous TiO_2 films, are affected by water vapor.

A further effect that strongly influences emf generation is the aging of $Pt/TiO_2/Ti$ samples. Samples that are not used directly after their preparation, i.e. stored in atmospheric air, must be subjected to a thermal activation treatment for 30s at a temperature of 700°C prior to attempting emf generation. The first plausible explanation that comes to mind is that the adsorption of atmospheric gases such as oxygen, water vapor and carbon dioxide may lead to the aging of the $Pt/TiO_2/Ti$ emf cells.

It is generally accepted that oxygen captures free electrons from TiO_2 surfaces during its adsorption and forms a large density of surface species such as O_2^-, O_2^{2-} and O_4^{2-} [34-37]. The O_2^- species has been found to be the most stable species on the surface of TiO_2 that desorbs as O_2 at temperatures above 410 K as reported by Henderson et al. [36].

The conductivity of polycrystalline thin TiO_2 films has been reported to decrease strongly in the presence of such oxygen-induced trap states located at the surfaces

and interfaces of grain boundaries [38]. Previously, a significant effect of oxygen on the Pt/TiO_2/Ti samples was shown by [39]. The samples were found to behave almost as isolators upon exposure to pure oxygen, most probably due to a large density of oxygen acceptor states at the Pt/TiO_2 interface that fix the Fermi level.

TiO_2 as a photocatalytic substrate is mainly used to reduce carbon dioxide during its adsorption on the surface. It is known that CO_2 is a rather inert molecule with a positive electron affinity of 0.6±0.2 eV [40], indicating that the reaction of CO_2 with electrons from TiO_2 to form CO_2^- anions is energetically unfavorable [41]. The interaction of CO_2 with the rutile TiO_2 (110) surface was investigated by Henderson [42] using the techniques of temperature programmed desorption (TPD), static secondary ion mass spectrometry (SSIMS), and high resolution electron energy loss spectrometry (HREELS). It was found that CO_2 binds weakly to the TiO_2 surface and preferentially to the oxygen vacancy sites. Furthermore, the presence of preadsorbed H_2O was observed to block CO_2 adsorption. Additionally, the adsorption of CO_2, with a relatively small binding energy of 0.56 eV [43] compared to the H_2O binding energy (0.64 eV) and O_2 binding energy (2.78 eV) on the vacancy site of TiO_2 [44], appears to have a negligible effect on aging, particularly in the presence of O_2 and H_2O.

In this study, we confirmed the existence of significant effects of temperature, water vapor and thermal activation on Pt/TiO_2/Ti emf cells:

i) Upon exposure to a hydrogen-in-air mixture, constant values of current densities up to 25 mA/cm^2 can be generated as long as the temperature is maintained at around room temperature via a suitable dissipation of the catalytically generated heat. If this condition is not met (for example, if the temperature rises to 65 °C) the generated current breaks down completely.

ii) It was found that adding water vapor to the hydrogen-in-air mixture not only reduces the effects of emf generation, but also reduces the catalytic oxidation of hydrogen on Pt.

iii) Pt/TiO_2/Ti samples stored in ambient air show a strong aging behavior which results in the generation of small emfs and current densities in a hydrogen-in-air mixture. However, flashing in air at 700 °C for 30s regenerates the aged samples to their initial active state.

We were able to extend the physiochemical emf model using microstructural investigations, microcalorimetry, current voltage (*I-V*) characteristics and electrochemical impedance spectroscopy (EIS) and thereby provide a basis for the optimal operating conditions for Pt/TiO_2/Ti emf cells.

Although Pt/TiO_2/Ti emf cells provide many inherent advantages over conventional single- and double-chamber fuel cells, their efficiency is very low. It is estimated to be approximately 2%. Similarly small values have been reported for single-chamber fuel cells [45]. A possible explanation for the low thermodynamic efficiency in our device may be that a large amount of unreacted hydrogen is exhausted from the measurement chamber. Therefore, further improvements, especially in terms of an optimized gas chamber design (demonstrator) with special facilities for gas flow, conversion of large amounts of hydrogen and a suitable dissipation of the catalytically generated heat and water, are needed to increase the efficiency of such cells.

The work described in this thesis consists of the three following chapters.

Chapter 1 presents the thermal properties of solid-state Pt/TiO_2/Ti emf cells. First, the temperature dependence of the generated current in a programmable gas flow system was investigated. Second, an isothermally operated microcalorimeter setup was used to determine various kinetic parameters such the rate of water formation, the reaction rate, and the activation energies of H_2 oxidation. These parameters provided information about the experimental determination of mass transport limitations and catalyst activity which, in turn, explains the thermal properties of Pt/TiO_2/Ti emf cells.

Chapter 2 focuses on the effect of water vapor on Pt/TiO_2/Ti emf cells. By means of current-voltage (*I-V*) characteristics and electrochemical impedance spectroscopy (EIS), the transport properties of Pt/TiO_2/Ti in humid air and in humid air with hydrogen were studied. A further experiment with microcalorimetry was performed to determine the H_2-to-H_2O turnover in the layer system of device. The data from the results provided an understanding of water vapor's effect on Pt/TiO_2/Ti emf cells.

In Chapter 3, the thermal activation of aged Pt/TiO_2/Ti emf cells was investigated. The aged samples, previously stored in atmospheric air, were subjected to a thermal activation treatment for 30s at a temperature of 700°C (a process known as flashing). Scanning electron microscopy (SEM), atomic force microscopy (AFM), Raman microscopy, X-ray photoelectron spectroscopy (XPS) and electrochemical impedance spectroscopy (EIS) were used to study aging's effect on the samples.

References

[1] Kakaç, S.; Pramuanjaroenkij, A.; Vasiliev, L. *Mini-Micro Fuel Cells: Fundamentals and Applications*; Springer, **2008**.

[2] Bagotsky, V. S., *Fuel cells: problems and solutions*; John Wiley & Sons, 2nd ed., 2011

[3] Kuhn, M.; Napporn T. W. Single-Chamber Solid Oxide Fuel Cell Technology-From Its Origins to Today's State of the Art; *Energies* **2010**, 3, 57-134.

[4] Schierbaum, K.; El Achhab M. Generation of an electromotive force by hydrogen-to-water oxidation with Pt-coated oxidized titanium foils. *Phys. Status Solidi A*, **2011**, .DOI 10.1002/pssa.201127400F.

[5] Ji, X. Z.; Somorjai, G. A. Continuous Hot Electron Generation in Pt/TiO_2, Pd/TiO_2, and Pt/GaN Catalytic Nanodiodes from Oxidation of Carbon Monoxide-Electron, *J. Phys. Chem. B* **2005**, 109, 22530-22535.

[6] Nienhaus, H. Electronic excitations by chemical reactions on metal surfaces, *Surf. Sci. Rep.* **2002**, 45, 1.

[7] Nienhaus, H.; Gergen, B.; Weinberg, W. H.; McFarland E. W. Detection of chemically induced hot charge carriers with ultrathin metal film Schottky contacts, *Surf. Sci.* **2002**, 514, 172.

[8] Nienhaus, H.; Bergh, H. S.; Gergen, B.; Majumdar, A.; Weinberg, W. H.; McFarland, E. W. Electron-Hole Pair Creation at Ag and Cu Surfaces by Adsorption of Atomic Hydrogen and Deuterium, *Phys. Rev. Lett.* **1999**, 82, 446-449.

[9] Park, J. Y.; Lee, H.; Renzas, J. R; Zhang, Y.; and Somorjai, G. A. Probing Hot Electron Flow Generated on Pt Nanoparticles with Au/TiO_2 Schottky Diodes during Catalytic CO Oxidation *Nano Lett.,* **2008**, 8, 2388-2392.

[10] Hervier, A.; Renzas J. R.; Park, J. Y.; Somorjai, G. A. Hydrogen Oxidation-Driven Hot Electron Flow Detected by Catalytic Nanodiodes, *Nano Lett*. **2009**, 9, 3930-3933.

[11] Yajima, T.; Koide, K.; Takai, H.; Fukatsu, N.; and Iwahara, H. Application of hydrogen sensor using proton conductive ceramics as a solid electrolyte to aluminum casting industries, *Solid State Ionics*, **1995,** 79, 333-337.

[12] Kunat, M.; Burghaus, U.; Wöll, C. The adsorption of hydrogen on the rutile TiO_2(110) surface. *Phys. Chem. Chem. Phys*. **2004**, *6*, 4203-4207.

[13] Suzuki S.; Fukui K.; Onishi H.; Iwasawa Y. Hydrogen Adatoms on TiO_2(110)-(1×1) Characterized by Scanning Tunneling Microscopy and Electron Stimulated Desorption, *Phys Rev Lett.* **2000**, 84, 2156-2159.

[14] Yin, X. L.; Calatayud, M.; Qiu, H.; Wang, Y.; Birkner, A.; Minot, C.; Woll, C. Diffusion Versus Desorption: Complex Behavior of H Atoms on an Oxide Surface. *ChemPhysChem* **2008**, 9, 253-256.

[15] Bates, J. B.; Wang, J. C.; Perkins, R. A. Mechanisms for Hydrogen Diffusion in TiO_2. *Phys. Rev. B*:. **1979**, 19, 4130-4139.

[16] Yerokhin, A.L.; Nie, X.; Leyland, A.; Matthews, A.; Dowey S.J. Plasma electrolysis for surface engineering. *Surf. Coat. Technol*. **1999**, 122, 73-93.

[17] Diamanti, M.V.; Pedeferri, M.P. Effect of anodic oxidation parameters on the titanium oxides formation. *Corros. Sci.* **2007**, 49, 939-948.

[18] Yerokhin, A.L.; Shatrov, A.; Samsonov, V.; Shashkov, P.; Pilkington, A.; Leyland, A.; Matthews, A. Oxide ceramic coatings on aluminium alloys produced by a pulsed bipolar plasma electrolytic oxidation process. *Surf. Coat. Technol*. **2005**, 199, 150-157.

[19] Rakoch, A.G.; Khokhlov, V.V.; Bautin, V.A.; Lebedeva, N.A.; Magurova, Y.V.; Bardin, I.V. Model concepts on the mechanism of microarc oxidation of metal materials and the control over this process. *Prot. Met.* **2006,** 42, 158-169.

[20] Kurze, P.; Krysmann, W.; Schneider, H.G. Applications fields of ANOF layers and composites. *Cryst. Res. Technol.* **1986**, 21, 1603-1609.

[21] Han, Y.; Hong, S.-H.; Xu, K.W. Porous nanocrystalline titania coatings by plasma electrolytic oxidation. *Surf. Coat. Technol.* **2002**, 154, 314-318.

[22] El Achhab, M.; Erbe, A.; Koschek, G.; Hamouich, R.; Schierbaum, K. A microstructural study of the structure of plasma electrolytically oxidized titanium foils. Appl. Phys. A **2014**, 116, 2039-2044.

[23] Sato, N., *Chemical Energy and Exergy: An Introduction to Chemical Thermodynamics for Engineers*, Elsevier, **2004**.

[24] Masel R. I. *Principles of Adsorption and Reaction on Solid Surfaces*; John Wiley & Sons, **1996**, p438.

[25] Gorodetskii, V. V.; Sametova, A. A.; Matveev, A. V.; Tapilin, V. M. From single crystals to supported nanoparticles in experimental and theoretical studies of H_2 oxidation over platinum metals (Pt, Pd): Intermediates, surface waves and spillover. *Catalysis Today* **2009**, *144*, 219-234.

[26] Wendt, S.; Matthiesen, J.; Schaub, R.; Vestergaard, E. K.; Lægsgaard, E.; Besenbacher, F.; Hammer, B. Formation and splitting of paired hydroxyl groups on reduced TiO_2(110). *Phys. Rev. Lett.* **2006**, *96*, 066107.

[27] Bikondoa, O.; Pang, C. L.; Ithnin, R.; Muryn, C. A., Onishi, H.; Thornton, G. Direct visualization of defect-mediated dissociation of water on TiO_2 (110). *Nature Materials* **2006**, *5*, 189-192.

[28] Ketteler, G.; Yamamoto, S.; Bluhm, H.; Andersson, K.; Starr, D. E.; Ogletree, D. F.; Ogasawara, H.; Nilsson, A.; Salmeron, M. The nature of water nucleation sites on TiO_2 (110) surfaces revealed by ambient pressure X-ray photoelectron spectroscopy. *J. Phys. Chem. C* **2007**, *111*, 8278-8282.

[29] English N. J. Dynamical properties of physically adsorbed water molecules at the TiO_2 rutile-(110) surface. *Chem. Phys. Lett.* **2013**, 583, 125-130.

[30] Zhang, C.; Lindan, P. J. D. Multilayer water adsorption on rutile TiO_2(110): A first-principles study *J. Chem. Phys*. **2003**, 118, 4620.

[31] Onda, K.; Li, B.; Zhao, J.; Jordan, K. D.; Yang, J.; Petek, H. Wet Electrons at the H_2O/TiO_2(110) Surface. *Science* **2005**, *308*, 1154-1158.

[32] Zhao, J.; Li, B.; Onda, K.; Feng, M.; Petek, H. Solvated Electrons on Metal Oxide Surfaces. *Chem. Rev*. **2006**, *106*, 4402-4427.

[33] Fischer, S. A.; Duncan, W. R.; Prezhdo, O. V. Ab Initio Nonadiabatic Molecular Dynamics of Wet-Electrons on the TiO_2 Surface. *J. Am. Chem. Soc*. **2009**, *131*, 15483-15491.

[34] Setvin, M.; Aschauer, U.; Scheiber, P.; Li, Y.-F.; Hou, W.; Schmid, M.; Selloni, A.; Diebold, U. Reaction of O_2 with Subsurface Oxygen Vacancies on TiO_2 Anatase (101). *Science* **2013**, 341, 988-991.

[35] Li, Y.-F.; Aschauer, U.; Chen, J.; Selloni, A. Adsorption and Reactions of O_2 on Anatase TiO_2. *Acc. Chem. Res.* **2014**, DOI: 10.1021/ar400312t.

[36] Henderson, M. A.; Epling, W. S.; Perkins, C. L.; Peden, C. H. F.; Diebold, U. Interaction of Molecular Oxygen with the Vacuum-Annealed TiO_2(110) Surface: Molecular and Dissociative Channels. *J. Phys. Chem. B* **1999,** *103*, 5328-5337.

[37] Pillay, D.; Wang, Y.; Hwang, G. S. Prediction of Tetraoxygen Formation on Rutile TiO_2(110). *J. Am. Chem. Soc.* **2006**, 128 (43), 14000–14001.

[38] Golego, N.; Studenikin, S. A.; Cocivera, M. Effect of oxygen on transient photoconductivity in thin-film $Nb_xTi_{1-x}O_2$, *Phys. Rev. B* **2000**, 61, 8262.

[39] Karpov, E. G.; Hashemian, M. A.; Dasari, S. K. Chemistry-Driven Signal Transduction in a Mesoporous Pt/TiO2 System. *J. Phys. Chem. C* **2013**, 117, 15632-15638.

[40] Compton, R. N.; Reinhardt, P. W.; Cooper, C. D. Collisional ionization of Na, K, and Cs by CO_2, COS, and CS_2: Molecular electron affinities *J. Chem. Phys.* **1975**, 63, 3821.

[41] Indrakanti, V. P.; Kubicki, J. D.; Schobert, H. H. Photoinduced activation of CO_2 on Ti-based heterogeneous catalysts: Current state, chemical physics-based insights and outlook. *Energy Environ. Sci.* **2009**, 2, 745.

[42] Henderson, M. A. Evidence for Bicarbonate Formation on Vacuum Annealed TiO_2(110) Resulting From a Precursor-Mediated Interaction Between CO_2 and H_2O. *Surf. Sci.* **1998**, 400, 203-219.

[43] Thompson, T. L.; Diwald, O.; Yates, J. T. CO_2 as a Probe for Monitoring the Surface Defects on TiO_2(110) Temperature-Programmed Desorption *J. Phys. Chem. B* **2003**, 107, 11700-11704.

[44] He, H.; Zapol, P.; Curtiss, L. A. A Theoretical Study of CO_2 Anions on Anatase (101) Surface. *J. Phys. Chem. C* **2010**, 114, 21474-21481.

[45] Shao, Z.; Haile, S. M; Ahn, J.; Ronney P. D.; Zhan, Z.; Barnett S. A. A thermally self-sustained micro solid-oxide fuel-cell stack with high power density. *Natur* **2005**, 435, 795-798.

Chapter 1

Thermal properties of solid-state $Pt/TiO_2/Ti$ emf cells studied with microcalorimetry

We have studied the temperature dependence of generated current during hydrogen-to-water oxidation over $Pt/TiO_2/Ti$ layer structures in which the oxide is grown by high-voltage electrochemical anodization of a titanium foil. The platinum contact is prepared using a paste process. We found that the generator effect breaks down completely at temperatures above 65 °C. By means of an isothermally operated microcalorimeter setup, the temperature dependence of the reaction was determined under flow conditions and evaluated in a thermodynamic constant-volume approach. Three different regimes can be distinguished between 1 and 157.3 °C in which the rate of reaction is controlled either by the activation energy of the reaction, the pore diffusion or the film diffusion. Based on the data, the thermal properties of solid-state $Pt/TiO_2/Ti$ emf cells are explained.

1.1 Introduction

Recent studies have shown an electromotive force (emf) generation during hydrogen-to-water oxidation over platinum coated anodized titanium foils [1,2]. To rationalize the overall phenomenon, we have suggested that the emf generation is caused by a spatial gradient of the partial pressure of H_2, and hence the chemical potential of hydrogen between platinum, at which H_2 is oxidized to H_2O, and titanium dioxide at or near the fringe of the Pt contact; at these sites hydroxylation of the surface and electron transfer to the supporting Ti foil has been postulated [1]. This model suggests that the hydrogen partial pressure at the titanium dioxide sites is higher than at platinum sites. Because of the large activity of platinum for the oxidation (see, e.g. [3]) one may expect that the vast majority of hydrogen is converted catalytically to water molecules during the diffusion through the Pt coating. Hence, it is obvious that direct catalytic oxidation of hydrogen competes with the emf generation path and reduces the efficiency of such cells. To quantitatively describe the emf effect in terms of yield, which is rate of electron release per time divided by the rate of H_2O formation [4], turnover

numbers for our system are required. The overall kinetics can be considerably distinct from single crystal data, particularly with regard to ambient pressure conditions and the porosity of platinum [5]. Apart from the specific temperature- and pressure-dependence, it is also a well-established feature of porous catalysts that gas-phase and pore diffusion as well as catalytic turnover are especially affected by structure; hence, to our knowledge an appropriate set of data is not available for our system.

In this paper, we first show the alteration of the generated current at different temperatures of hydrogen-to-water oxidation by platinum coated anodized titanium foils and then we present an experimental approach to determine various kinetic parameters including pore diffusional rates, turnover numbers and activation energies of H_2 oxidation. By identifying these parameters, the experimental determination of the mass transport limitations and activity of the catalyst are achieved. This in turn explains the thermal properties of emf cells.

1.2 Experimental

1.2.1 Sample preparation

Two kind of samples (10×10 mm^2, type-I, and 1.5×9.5 mm^2, type-II) were prepared according to the method described in [1, 6]. The porous TiO_2 layer was formed electrochemically and the porous Pt layer was fabricated in a paste process. The area of platinum on the type-I sample, which was used to show the temperature dependence of the generated current, was 5×5 mm^2. The surface of the sample type-II, used for the microcalorimetric study, was completely coated with Pt [6].

1.2.2 Experimental setup

We used a programmable gas-flow system with mass-flow controllers to adjust the overall gas flow and the concentration of hydrogen.

The chamber for microcalorimetric measurements is surrounded with a double-walled box; a short rifled tube and a further ¼ inch pipe, brazed in two adjacent

bores of the chamber, form the inlet and outlet for the gas flow, respectively. The rifled tube at the inlet, encircled by the cooling liquid of a refrigerated circulator (FP50, Julabo), improves the heat exchange with the gas mixture flowing through the chamber. The measurement chamber, a hollow cylinder with an internal volume of 6 cm^3 made of copper, is equipped with a single KF16 flange for installing the calorimetric device. It consists of a microheater (Pt 6,8 M 1020, Heraeus) and a Pt100 resistor (Pt 222, Heraeus), stuck together and mounted on an electrical feedthrough (C9-K16, Caburn-MDC). The $Pt/TiO_2/Ti$ sample type-I is attached to the reverse of the microheater by means of silver conductive paint. The heater and the Pt100 resistor are part of a temperature control system that consists of a PID controller (4100 plus, West) and a power supply (VSP1410, Voltcraft). The transient of the electrical power, dissipated at the microheater to maintain a constant temperature in the gas flow, is determined by means of digital current and voltage meters (8808A, Fluke).

The second chamber, which is made of Pyrex glass with an internal volume of 1.3 cm^3, is used to measure the generated current of $Pt/TiO_2/Ti$ structures. The internal volume, which contains the sample and the electrical connections to the Pt coating and the Ti foil, is connected to ¼ inch pipes through which the H_2/air mixture flows. The chamber is fixed with two screws on a stainless steel body that is also connected to the refrigerated circulator which enables heating or cooling of the sample at a constant temperature. The transients of generated current are determined with a digital multimeter (8808A, Fluke). All instruments are operated from a LabVIEW platform that also collects all relevant experimental data.

1.3 Results

Figure 1 shows the transient of the generated current obtained upon exposure to a 3.5 vol.-% concentration of hydrogen at 20 °C, 40 °C, and 65 °C. Constant and high values of the current densities up to 25 mA/cm^2 can be generated with the $Pt/TiO_2/Ti$ sample at around room temperature over a long period of time during exposure to H_2/air mixtures. Upon slowly increasing the temperature to 40 °C, the

current initially rises but above 30 °C it decreases until it becomes constant at a current density of 18 mA/cm^2. But, if the temperature of the sample rises to 65 °C, the generated current breaks down completely, as can be seen in Figure 1. In ref [7], the authors reported on a similar temperature effect on reaction current in mesoporous Pt/TiO_2 structures. Distinct processes such as the change in the chemical reaction rate and change in the efficiency of detection of the excited charge carries were suggested as explanations. In this work, we used microcalorimetry to investigate the chemical reaction rates during the hydrogen-to-water oxidation over solid-state Pt/TiO_2/Ti emf cells.

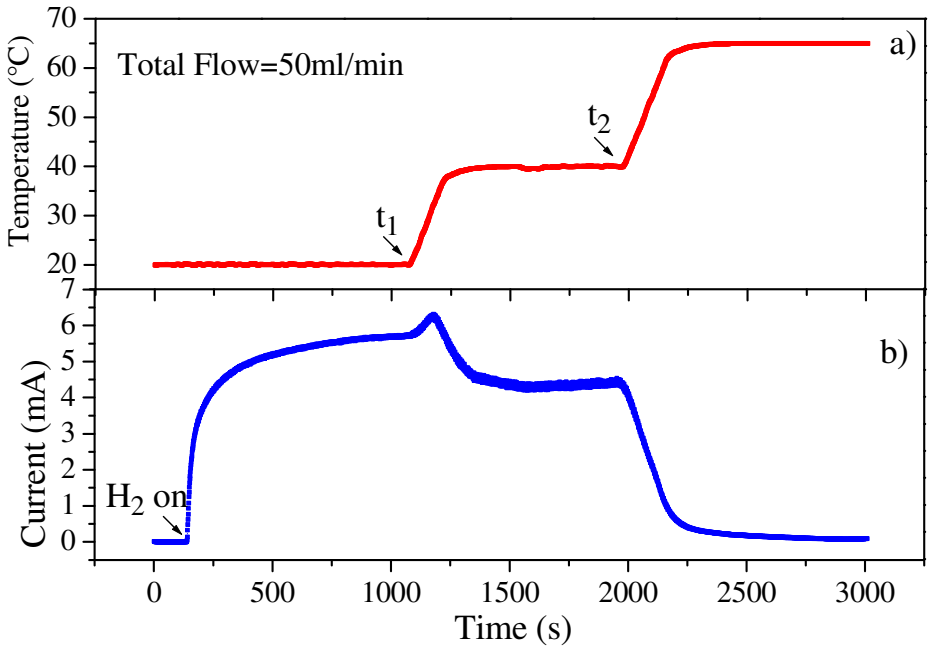

Figure 1. Transient of the temperature (red curve) of the type-I sample (a). At t_1 (t_2), the sample is heated to 40 °C (65 °). The transient of the generated current is shown by the blue curve at a constant H_2 fraction of 3.5 vol.-%in air (b).

For these experiments, pure air flows with a constant volume flow rate over the sample; a constant temperature *T* is maintained by electrical power dissipation in the microheater, balancing the heat transfer to the surroundings. Hydrogen-containing air is added so that volume flow rates remain constant and volume fractions of H_2 between 0.5 and 3.5 vol.-% are employed consecutively. The

duration of each exposure is 300 s. To prevent an increase of T in the low temperature regime in which the heat release of the exothermic hydrogen oxidation on the sample exceeds the electrical power, the gas phase and the measurement chamber is cooled to a constant value of -30 °C. Figure 2 shows the transient of the electrical power at various sample temperatures between 1 °C, i.e. just above the freezing point of water, and 157.3 °C. As the result oexothermic reaction the electrical power decreases immediately after exposing the samples to hydrogen. The effect is detectable with our instruments even at low H_2 volume fractions of about 1000 ppm. The constant values of P in the initial phase (0…600 s) equal the heat transfer to the surroundings; these values are also used in the following analysis.

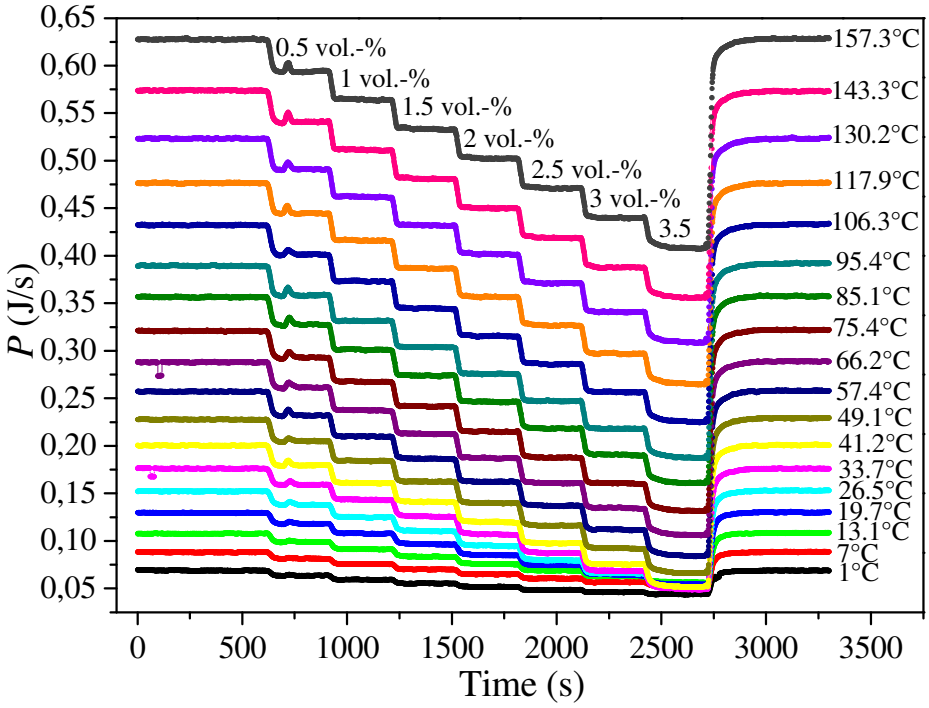

Figure 2. Electrical power P, consumed by the microheater to maintain a constant temperature, as a function of time t for stepwise increase of the hydrogen volume fraction in air. Each transient has been shifted to time zero for simplification.

1.4 Discussion

Considered thermodynamically, the measuring cell in flow apparatus reflects a one-inlet one-exit control volume with one-dimensional gas flow (Figure. 3) for which the energy rate balance equation is known from the conversation of energy principle [8].

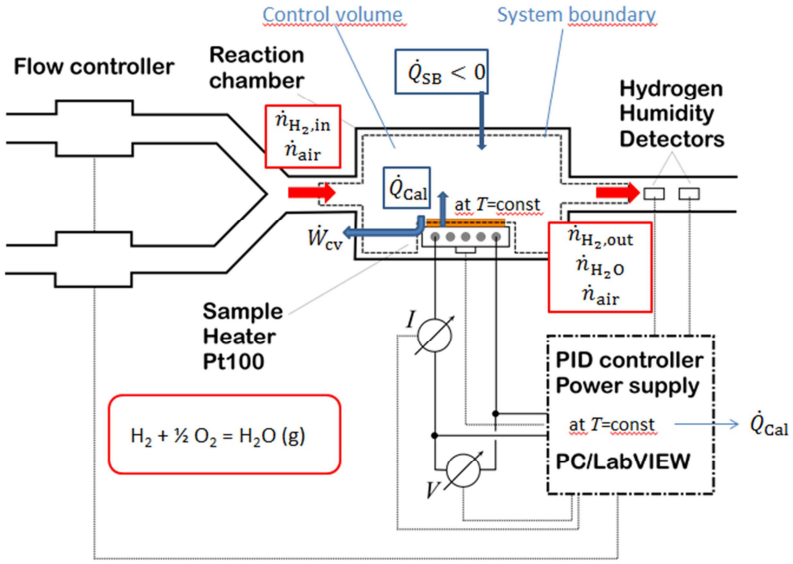

Figure 3. Schematic representation of the control volume enclosing the measurement chamber.

In our case we can neglect potential and kinetic energy effects since the gravitational potential energies at the inlet (in) and outlet (out) of the test chamber are the same. Likewise, there is no significant difference in the kinetic energies and velocities of the gas flow at the inlet and the exit. $\dot{Q}_{CV}$ describes the entire heat flux ("heat exchange rate", with unit J/s) through the system boundary between the environment and the control chamber, and $\dot{W}_{CV}$ is the electrical power generated by the Pt/TiO_2/Ti sample during H_2 oxidation. In this work, we use the following sign convention for heat and work transfer into and from a system to ensure the consistency with the first law of thermodynamics: heat transfer is taken to be positive if flux occurred in the direction of the arrows in Figure 3 and negative otherwise.

We separate $\dot{Q}_{CV}$ into two parts:

$$\dot{Q}_{\mathrm{CV}} = \dot{Q}_{\mathrm{Cal}} + \dot{Q}_{\mathrm{SB}} \tag{1}$$

where $\dot{Q}_{\mathrm{Cal}}$ denotes the heat flux to/from the microcalorimeter, and $\dot{Q}_{\mathrm{SB}}$ is the heat flux across the system boundary to the environment. In our experiments, the latter is negative ($\dot{Q}_{\mathrm{SB}} < 0$), whereas $\dot{Q}_{\mathrm{Cal}} \geq 0$.

The only mode in which the work is exchanged between the control chamber and the environment is electrical, namely EMF generation. A good approximation of this is:

$$\dot{Q}_{\mathrm{CV}} \gg \dot{W}_{\mathrm{CV}} \tag{2}$$

A chemical reaction (oxidation) of H_2 to H_2O (water vapor) will occur in the control chamber. However, this reaction cannot be completed so that both unconsumed H_2 and the vapor appear at the outlet at rates $\dot{n}_{\mathrm{H_2,out}}$ and $\dot{n}_{\mathrm{H_2O}}$. The change of the rate $\dot{n}_{\mathrm{air}} = \dot{n}_{\mathrm{air,in}} = \dot{n}_{\mathrm{air,out}}$ and the (average) molecular weight M can be neglected, since O_2 is used in excess. The amount of substance balance can be written:

$$\dot{n}_{\mathrm{H_2,in}} = \dot{n}_{\mathrm{H_2,out}} + \dot{n}_{\mathrm{H_2O}} \tag{3}$$

In the stationary case, the energy balance equation is:

$$\dot{Q}_{\mathrm{CV}} - \dot{W}_{\mathrm{CV}} + \dot{n}_{\mathrm{H_2,in}}\bar{h}_{\mathrm{H_2}}\left(T, p_{\mathrm{H_2}}\right) - \dot{n}_{\mathrm{H_2,out}}\bar{h}_{\mathrm{H_2}}\left(T, p_{\mathrm{H_2}}\right) - \dot{n}_{\mathrm{H_2O}}\bar{h}_{\mathrm{H_2O}}\left(T, p_{\mathrm{H_2O}}\right) = 0 \tag{4}$$

where $\bar{h}_{\mathrm{H_2}}\left(T, p_{\mathrm{H_2}}\right)$ and $\bar{h}_{\mathrm{H_2O}}\left(T, p_{\mathrm{H_2O}}\right)$ are the specific molar enthalpies of hydrogen and water at temperature T and respective partial pressures p. The work rate $\dot{W}_{CV}$ can be neglected due to inequality (2).

H_2 and H_2O are treated as ideal gases at states under experimental conditions, dry air as a pure component and mixtures of them in air as an ideal gas mixture which can be verified by reference to appropriate property data; it follows from calculation of the reduced temperature and pressure from the critical data and a comparison with the generalized compressibility chart. As a consequence, the

molar enthalpy $\bar{h}(T,p)$ with respect to the molar enthalpy at the pressure p_{ref} =1.013 bar in the reference condition, given as

$$\bar{h}(T,p) = \bar{h}(T,p_{\mathrm{ref}}) + \int_{p_{\mathrm{ref}}}^{p}\left[\bar{v} - T\left(\frac{d\bar{v}}{dT}\right)_p\right]dp = \bar{h}(T,p_{\mathrm{ref}}) \tag{5}$$

is independent of pressure since the integral term in equation (5) cancels out for an ideal gas. In Equation (5), $\bar{v} = RT/p$ is the molar volume. The temperature-dependence of the molar enthalpies is expressed by

$$\bar{h}(T,p_{\mathrm{ref}}) = \bar{h}(T_{\mathrm{ref}},p_{\mathrm{ref}}) + \int_{T_{\mathrm{ref}}}^{T} c_p(T)dT \tag{6}$$

with the reference temperature T_{ref} = 298.15 K. Constant ideal gas specific heats c_p can be used for a good approximation: c_p= 3.5R for H_2 and c_p= 4R for H_2O (R is gas constant = 8.314 J/mol·K). The molar enthalpies are then given by

$$\bar{h}_{\mathrm{H_2}} = \bar{h}_{\mathrm{f}}^{\mathrm{o}}(\mathrm{H_2}) + 3.5R(T - T_{\mathrm{ref}}) \tag{7a}$$

$$\bar{h}_{\mathrm{H_2O}} = \bar{h}_{\mathrm{f}}^{\mathrm{o}}\left(\mathrm{H_2O_g}\right) + 4R(T - T_{\mathrm{ref}}) \tag{7b}$$

with molar standard enthalpies $\bar{h}_{\mathrm{f}}^{\mathrm{o}}(\mathrm{H_2})$= 0 for the element gas H_2 and $\bar{h}_{\mathrm{f}}^{\mathrm{o}}\left(\mathrm{H_2O_g}\right)$ = -241.820 kJ/mol for steam [6].

Thus, together with the above assumptions, $\dot{Q}_{Cal}$ can be written as follows:

$$\dot{Q}_{\mathrm{Cal}} = \dot{n}_{\mathrm{H_2O}}\left(\bar{h}_{\mathrm{f}}^{\mathrm{o}}\left(\mathrm{H_2O_g}\right) + \tfrac{1}{2}R(T - T_{\mathrm{ref}})\right) - \dot{Q}_{\mathrm{SB}} \tag{8}$$

$\dot{Q}_{\mathrm{SB}}$ can be determined by a "blind" measurement without H_2. In this case, $\dot{n}_{\mathrm{H_2O}}$ = 0 holds and Eq. (8) simplifies to

$$\dot{Q}_{\mathrm{Cal}} = -\dot{Q}_{\mathrm{SB}}. \tag{9}$$

Values of $\dot{Q}_{\mathrm{SB}}$ can be determined from the baseline of the transients in Figure 2.

The rate $\dot{n}_{\mathrm{H_2,in}}$ is calculated assuming

$$\dot{n}_{\mathrm{H_2,in}} = y_{\mathrm{H_2}} \dot{n}_{\mathrm{air}} \tag{10}$$

where $y_{\mathrm{H_2}}$ is a molar fraction of hydrogen in % or ppm in air. The rate $\dot{n}_{\mathrm{air}}$ is given by

$$\dot{n}_{\mathrm{air}} = (p\dot{V})/(RT) \tag{11}$$

where p = 1.013 bar, and $\dot{V}$ denotes volume flow rate in m^3/s, here 50 ml/min = 8.3×10^{-7} m^3/s. Results of $\dot{Q}_{\mathrm{Cal}}$ as a function of $\dot{n}_{\mathrm{H_2,in}}$ and sample temperature are shown in Figure 4. Equation (8) allows for the calculation of $\dot{n}_{\mathrm{H_2O}}$ from $\dot{Q}_{\mathrm{Cal}}$. The temperature-dependent term is small compared with the molar standard enthalpy of steam, and hence we can write to a good approximation

$$\dot{n}_{\mathrm{H_2O}} \approx \frac{\dot{Q}_{\mathrm{Cal}} + \dot{Q}_{\mathrm{SB}}}{-241\ \mathrm{kJ/mol}} \tag{12}$$

The evaluation of the experimental data yields the turnover relationship $\dot{n}_{\mathrm{H_2O}} = f(\dot{n}_{\mathrm{H_2,in}})$ for the Pt/TiO_2/Ti system; results are plotted in Figure 5.

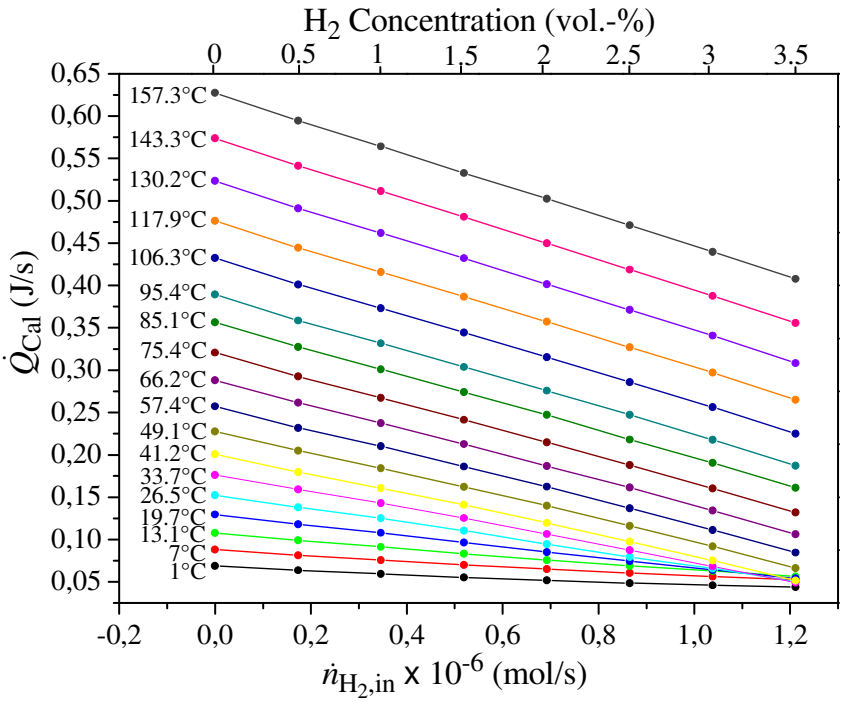

Figure 4. Values of $\dot{Q}_{\mathrm{Cal}}$ as a function of the hydrogen flow $\dot{n}_{\mathrm{H_2,in}}$ in at different sample temperatures.

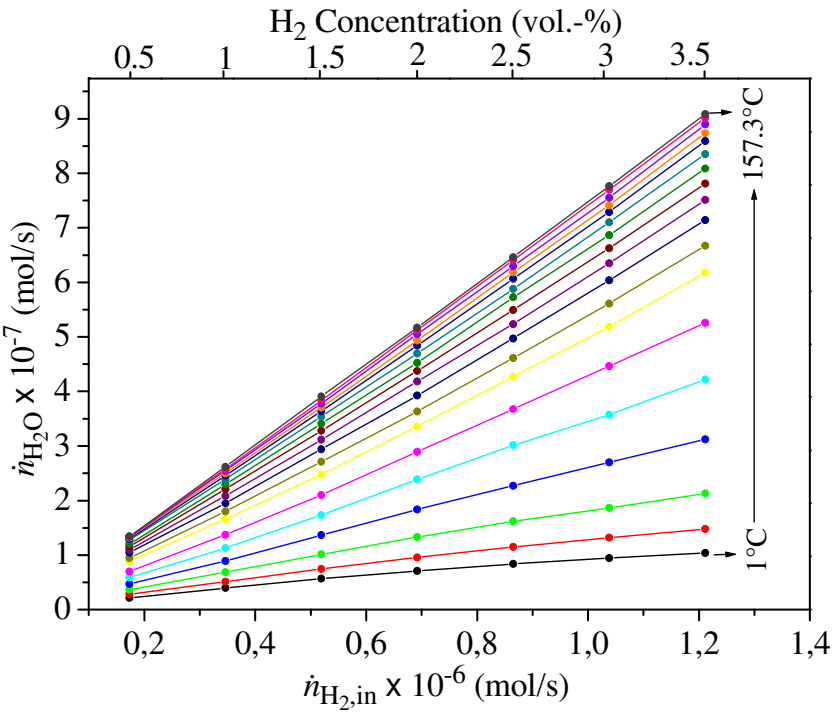

Figure 5. Rate of water formation $\dot{n}_{H_2O}$ as a function of the hydrogen flow $\dot{n}_{H_2,in}$ at different sample temperatures.

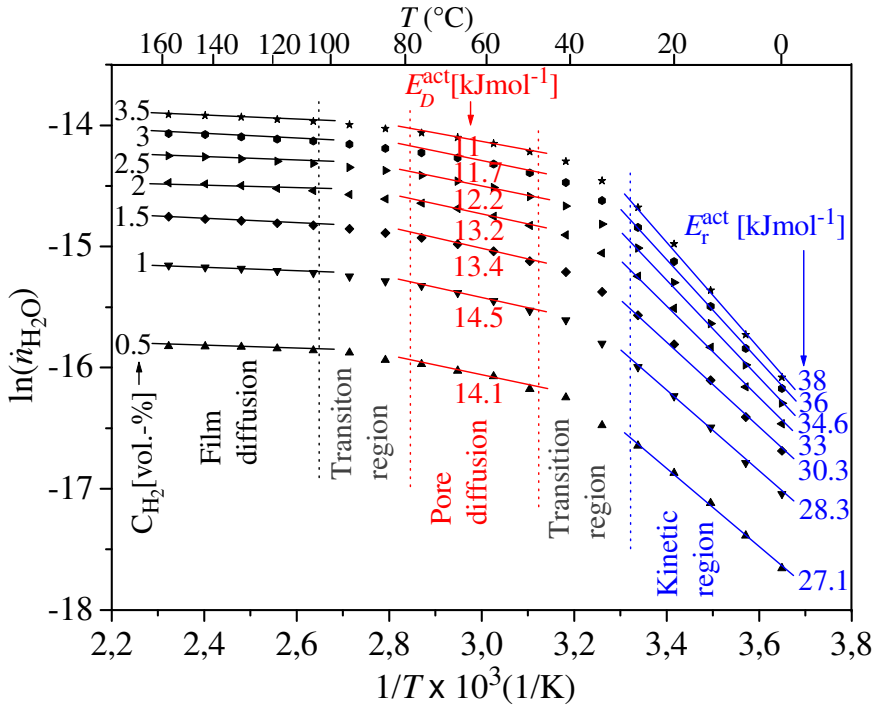

Figure 6. Temperature dependence of reaction rate of H_2O occurring in $Pt/TiO_2/Ti$ sample.

The graphs in Figure 5 reflect the considerable boosting influence of the temperature on turnover numbers between 1 °C and 30 °C and only minimal thermal effects on $\dot{n}_{H_2O}$ above approximately 100 °C.

For graphical analysis of the temperature dependence, the experimental values $\dot{n}_{H_2O}$ are plotted as a function of reciprocal temperature ($1/T$) in an Arrhenius diagram, which represents three different regimes (Figure 6). In the low-temperature regime we determine the activation energy E_r^{act} of the reaction by evaluating

$$\dot{n}_{H_2O} \sim k = A\exp\left(\frac{E_r^{act}}{RT}\right), \tag{13}$$

where k and A denote the rate constant and frequency factor, respectively. The value of E_r^{act} rises from 27.1 kJ/mol at a low H_2 flux to 38 kJ/mol for the highest flux applied in our experiment. The frequency factors cannot be derived from our measurements. The activation energies, attributed to the intrinsic kinetics of the Pt-catalyzed hydrogen oxidation, are lower than 50 kJ/mol [9] and 67 kJ/mol [10]. As suggested by Wintterlin, the autocatalytic effect of adsorbed water, found in a scanning tunneling microscopy and high-resolution electron energy loss spectroscopy study on Pt(111), cannot be ruled out for “real” catalysts at temperatures well above the desorption temperature of H_2O at 170 K [11], which may lead to the observed deviation from literature values.

Around room temperature (kinetic region) the film and pore diffusion of H_2 and O_2 proceed quickly and are not rate-determining: we assume therefore that the reactants may penetrate to the titanium dioxide sites without being completely converted to water on their way. Consequently, a constant and high value of the generated current at room temperature is observed. At 40 °C we find a regime at which the transport of the reactants in the pore system of platinum becomes rate-determining. This is in correspondence with the observed drop in the current transient at 40 °C (Figure 1).

For pore diffusion we observe activation energies $E_{\mathrm{p}}^{\mathrm{act}}$ in the kinetic region for the concentrations above 2 vol.-%, which are roughly half of the values $E_{\mathrm{r}}^{\mathrm{act}}$. Our findings are hence consistent with the theory that predicts a temperature-dependence of rate

$$r \sim \exp\left(-\frac{E_{\mathrm{r}}^{\mathrm{act}}+E_{\mathrm{D}}^{\mathrm{act}}}{2RT}\right) \approx \exp\left(-\frac{E_{\mathrm{r}}^{\mathrm{act}}}{2RT}\right) \tag{14}$$

for isothermal pore diffusion, in which the effective activation energy of diffusion $E_{\mathrm{D}}^{\mathrm{act}}$ almost fails to contribute due to its small value [12].

Because of the high oxidation rate for T > 50 °C, we may assume that the local concentration at the Pt surface is almost zero; the reactants are almost completely converted at the external surface of the catalyst without reactants reaching the titanium dioxide, which may be the main reason for the breakdown of the generated current at 65 °C.

Figure 6 also illustrates the limiting effect of external mass transfer (film diffusion) on activation energy. At temperatures above approximately 100 °C the activation energy of the reaction in the film diffusion region becomes small. This regime does not play a significant role for the emf cell because no current is generated.

1.5 Conclusions

In this work, measurements of the generated current and a microcalorimetric study were carried out on Pt/TiO_2/Ti emf cells during hydrogen-to-water oxidation. In accordance with earlier measurements [1], we confirmed the drastic temperature dependence of the generated current. We could correlate the thermal properties with the temperature dependence of the hydrogen-to-water oxidation as measured with microcalorimetry. As long as the temperature is maintained in the kinetic region by a suitable dissipation of the catalytically generated heat, constant and high values of the generated current can be generated. This may be related to sufficient transport of the reactants through the pores of Pt to the titanium dioxide

sites. If this condition is not met (e.g., if the pore diffusion is rate-determining, i.e. above 50 °C), the emf effect breaks down completely.

1.6 References

[1] Schierbaum, K.; El Achhab M. Generation of an electromotive force by hydrogen-to-water oxidation with Pt-coated oxidized titanium foils. *Phys. Status Solidi A* **2011**, .DOI 10.1002/pssa.201127400F.

[2] Karpov, E. G.; Hashemian, M. A.; Dasari, S. K. Chemistry-Driven Signal Transduction in a Mesoporous Pt/TiO_2 System. *J. Phys. Chem. C* **2013**, 117, 15632-15638.

[3] Sachs C.; Hildebrand M.; Völkening S.; Wintterlin J.; Ertl G. Reaction fronts in the oxidation of hydrogen on Pt(111): Scanning tunneling microscopy experiments and reaction–diffusion modelling. *J. Chem. Phys*. **2002,** 116, 5759.

[4] Hervier A.; Renzas J. R; , Park J. Y.; Somorjai G. A. Hydrogen oxidation-driven hot electron flow detected by catalytic nanodiodes. *Nano Lett*. **2009,** 9, 3930.

[5] Ikeda H.; Sato J.; Williams F.A. Surface kinetics for catalytic combustion of hydrogen-air mixtures on platinum at atmospheric pressure in stagnation flows. *Surf. Sci.* **1995,** 326, 11-26.

[6] El Achhab, M.; Erbe, A.; Koschek, G.; Hamouich, R.; Schierbaum, K. A microstructural study of the structure of plasma electrolytically oxidized titanium foils. *Appl. Phys. A* **2014**, *116*, 2039-2044.

[7] Hashemian, M. A.; Palacios, E.; Nedrygailov, I. I.; Diesing, D.; Karpov, E. G. Thermal Properties of the Stationary Current in Mesoporous Pt/TiO_2Structures in an Oxyhydrogen Atmosphere. *ACS Appl. Mater. Interfaces* **2013**, *5*, 12375-12379.

[8] Moran M. J.; Shapiro H. N. (eds.). Fundamentals of Engineering Thermodynamics (John Wiley & Sons, **2008**, p. 156.

[9] Smith J. N.; Palmer R. L. Molecular Beam Study of the Oxidation of Deuterium on a (111) Platinum Surface. *J. Chem. Phys*. **1972,** 56, 13.

[10] Anton A. B.; and Cadogan D. C. The mechanism and kinetics of water formation on Pt(111). *Surf. Sci*. **1990,** 239, L548-L560.

[11] Völkening S.; Bedürftig K.; Jacobi K.; Wintterlin J.; Ertl G Dual-Path Mechanism for Catalytic Oxidation of Hydrogen on Platinum Surfaces. *Phys. Rev,Lett.* **1999,** 83, 2672.

[12] Dittmeyer R.; and Emig G. Simultaneous Heat and Mass Transfer and Chemical Reaction, in: Ertl G.; Knözinger H.; Schüth F.; Weitkamp J. (eds.), Handbook of Heterogeneous Catalysis Vol. 3 (Wiley & VCH-Verlag, **2008**, p. 1727.

Journal: Applied Physics A: Materials Science & Processing

Impact Factor: 1.44

Own contribution: 75%

1. Author

Chapter 2

The Effect of Water Vapour on Pt/TiO_2/Ti Emf Cells

We study the humidity dependence of the generated current of Pt/TiO_2/Ti electromotive force (emf) cells by means of microcalorimetry, current voltage (I-V) characteristics and electrochemical impedance spectroscopy (EIS). We prepare TiO_2 with a high-voltage electrochemical anodisation and the Pt electrode via a paste process. We find that short circuit current densities (J_{sc}) significantly vary by adding water vapour to the 2.1 vol% hydrogen-in-air mixture used to generate the emf, while the open-circuit voltage (V_{oc}) always increases with increasing relative humidity (RH); J_{sc} increases from 8.2 mA/cm^2 (RH = 0 %) to a maximum value of 9.4 mA/cm^2 (RH = 10 %). At RH > 10 %, J_{sc} decreases slightly. The increase in J_{sc} is interpreted as enhanced electron transport as a consequence of the interaction of water with TiO_2, while the decrease in J_{sc} seems to be related to a large amount of water negatively affecting the rate-determining step for emf.

2.1 Introduction

Single-chamber fuel cells offer a simpler design than conventional fuel cells since they do not require a separate fuel and oxidiser supply [1]. Current concepts are based on high-temperature solid ion conduction, operated between 500 and 950 °C, and reach electrical power densities up to a few hundred mW/cm^2 [2,3]. More recently, microbial fuel cell designs were investigated [4]. A solid-state room temperature approach was presented in Ref. [5] that makes use of the generation of an electromotive force (emf) during the hydrogen oxidation over Pt/TiO_2/Ti structures [6,7]. The results of our previous study with microcalorimetry indicate that a large number of water molecules are formed via catalytic oxidation of H_2 during emf generation [8]. It is well known that water interacts with TiO_2 [9-17] and water affects hydrogen-to-water oxidation over Pt catalysts [18-19]. For the Pt/TiO_2/Ti system, the question remains whether the current density is affected by water vapour which is added to the H_2/air mixture.

In this work, we first show the effect of water vapour on the current-voltage characteristics of Pt/TiO_2/Ti emf cells. Then, we use microcalorimetry and

electrochemical impedance spectroscopy to study the catalytic behaviour of the porous Pt contact and transport properties of $Pt/TiO_2/Ti$. The results suggest an interpretation of the water vapour effect on $Pt/TiO_2/Ti$ emf cells.

2.2 Experimental Details

A titanium foil (99.6 % purity; 10×10 mm^2 and 125 µm thick) was anodically oxidised at 150 V according to the recipe in Ref. [20] to yield mesoporous titanium dioxide. The oxidised Ti foil was subsequently washed in deionised water and then dried at 100 °C for 1 min. For the top electrode, a platinum paste (Chempur 900487) was applied to the surface of the oxide. The Pt area was 7×7 mm^2. The surface of the microheater (1.5×9.5 mm^2), used for the calorimetric setup, was completely coated with Pt paste. Both the $Pt/TiO_2/Ti$ sample and the microheater with the Pt coating were heat-treated at 700 °C for 30 s prior to mounting them in the measurement chamber.

The experiments were performed in a gas-flow apparatus with two pressurised gas bottles (3.5 vol.% H_2 in synthetic air and synthetic air only). Details are described in Ref.[8] A fraction of 2.1 vol% H_2 in air was adjusted by mixing appropriate fluxes from both bottles. To alter the humidity between 0 % and 40 %, part of the pure dry air was conducted through liquid water in a gas washing bottle. All experiments were carried out at a total flux of 100 ml/min and at room temperature. At this temperature, the adjusted humidity corresponds to 0.23 vol% (RH = 10 %), 0.46 (20 %), 0.69 (30 %) and 0.92 (40 %) H_2O vapour in air. The duration of each exposure was 600 s. The *I-V* characteristics and the electrochemical impedance spectra (EIS) were determined using an Autolab instrument (PGSTAT302N, Metrohm) combined with a FRA32M module. The amplitudes of AC signal and DC bias voltage were set at 20 mV and zero, respectively.

2.3 Results and discussion

Figure 1 displays a series of *I-V* curves for the $Pt/TiO_2/Ti$ sample in a voltage range between -0.8 V and +0.8 V. The $Pt/TiO_2/Ti$ sample was initially exposed

to 2.1 vol% H_2 in dry air. We calculated a short circuit current density (J_{sc}) of 8.2 mA/cm^2 from the measured current I_{sc} and the contact area. Under this condition, the open circuit voltage equals 0.36 V. At RH = 10 %, the current density J_{sc} rises to 9.4 mA/cm^2. Further increasing the humidity to 20 % results in a decreased value of J_{sc} of 8 mA/cm^2. Above 20 % J_{sc}, decreases markedly. Interestingly, the open circuit voltage V_{oc} always increases with increasing humidity, as shown in Figure 1. Numerous Pt/TiO_2/Ti samples were prepared and the generator effect has been found to be reproducible with similar current density increases upon additional exposure to humidity between RH = 0 and 20 %. Note the strong reduction in current in the reversed and forward bias regime of the *I-V* characteristics with increasing humidity.

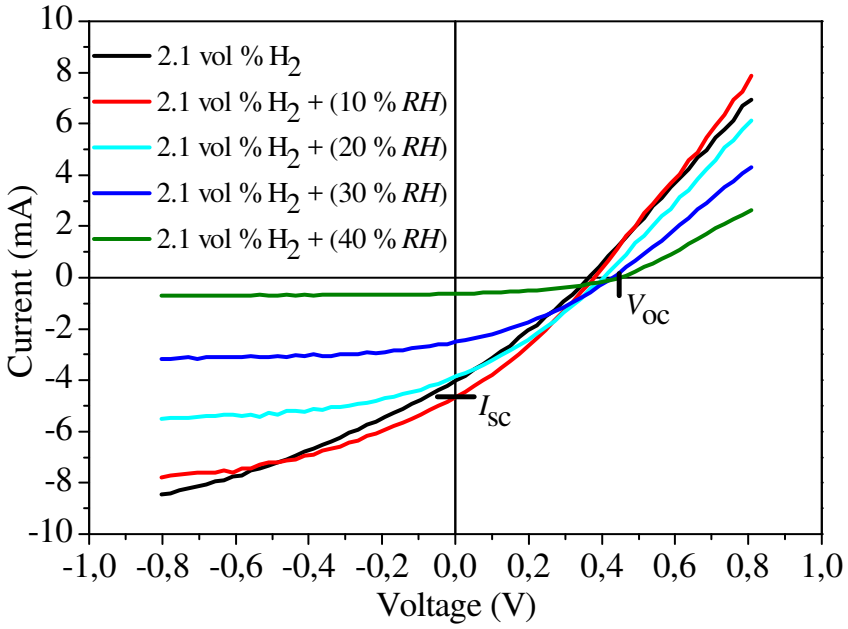

Figure 1. The evolution of the *I-V* curves of Pt/TiO_2/Ti at 2.1 vol% H_2 in dry and humid air.

Next, we investigated whether the catalytic turnover of hydrogen to water occurring at the Pt/TiO_2/Ti layer structure reveals a similar volcano-type feature if humidity changes. To do this, we used the microcalorimeter setup described in detail in Ref.[4] Measurements were carried out using identical gas mixtures in the same temporal sequence of exposures as given in Figure 1.

Figure 2 shows the electrical heating power of the microheater as a function of time. In the initial period (0-300 s), the observed power corresponds to the value required to maintain a constant temperature of 20 °C. The exterior of the measurement chamber was maintained at a constant temperature of 5 °C to enable efficient temperature regulation. During hydrogen exposure at 300 s, the power decreases, because the reaction heat of the H_2-to-H_2O oxidation is released. The decrease in P equals the heat production rate $\dot{Q}$. After 900 s, the humidity was changed. At RH = 10 %, the electrical power initially drops before increasing again until it becomes constant; this is due to switching off the mass flow controllers and mixing the gas flow through the water container. As can be seen from the data in Figure 2, the rate $\dot{Q}$ decreases at RH > 0 %**.** This result suggests that H_2-to-H_2O turnover decreases if additional water vapour is present with a gradual decrease of $\dot{Q}$. No maximum was found at 10 % RH as compared to the behaviour of J_{sc}. Furthermore, hysteresis effects were found during increasing and decreasing of the humidity. Slightly smaller steady state values of the electrical power (not shown) were observed for reverse direction (40% to 0 % RH) in comparison to the values obtained in forward direction (0 % to 40 % *RH*).

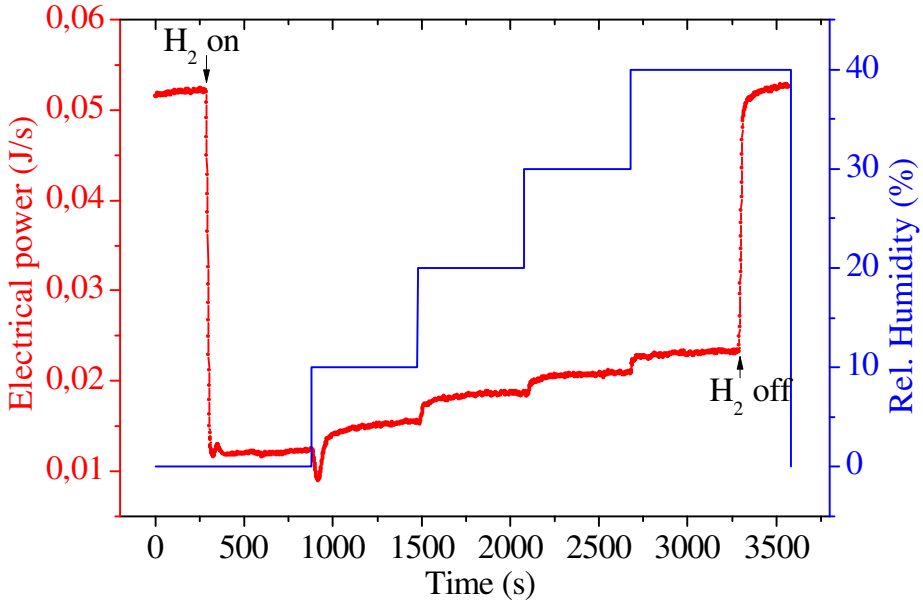

Figure 2. The effect of humidity on hydrogen oxidation on Pt (red curve). The blue curve represents the variation of relative humidity.

To explore the effect of humidity on Pt/TiO_2/Ti without hydrogen, the *I-V* characteristics were determined in dry air after changing the relative humidity from 10 % to 40 %. As shown in Figure 3, the Pt/TiO_2/Ti sample is almost insulated over the entire voltage range of -0.8 to +0.8 V in dry air at room temperature. This shows that the applied voltage has almost no effect on band bending at the Pt/TiO_2 interface, in line with the earlier reports, [6,7] most likely due to a large number of oxygen acceptor states that fix the Fermi level. It is generally accepted that O_2 traps negative charge during adsorption on TiO_2 [21].

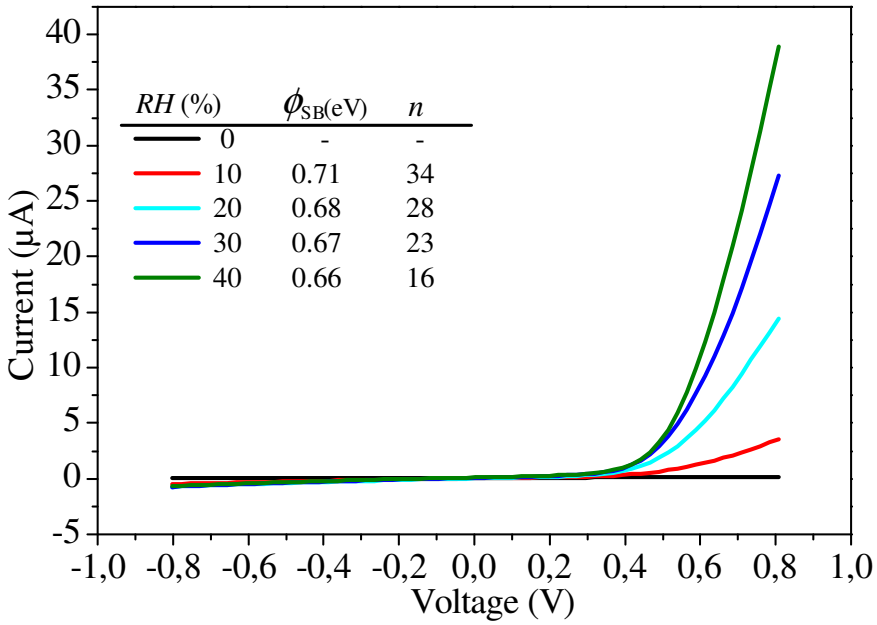

Figure 3. *I-V* characteristics of Pt/TiO_2/Ti structure in dry and humid air. The inset table shows values for Schottky barrier height and ideality factor. Further explanations are given in the text.

Schottky barrier heights ϕ_{SB} and ideality factors *n*, obtained by fitting (using equation (2) in Ref. [22]), decrease from 0.71 eV (34) at *R*H = 10 % to 0.66 eV (16) at RH = 40 % (see inset in Figure 3). The data are consistent with the assumption that the increased adsorption of H_2O molecules gradually reduces the density of the oxygen-derived surface states at the interface, but even at 40 % *RH* the Schottky barrier between Pt and TiO_2 remains.

Next, impedance spectroscopy was performed to obtain information about charge transport and relaxation properties that might occur in Pt/TiO_2/Ti. Such effects depend on the timescale over which ionic and electronic species respond to an external AC signal. Sets of impedance spectra Z'-*vs*-Z'' were taken at no bias voltage (i.e. V = 0) in dry and humid air with hydrogen in a frequency range between 1MHz and 25Hz and without hydrogen in a frequency range between 1MHz and 0.1Hz (Figure 4).

In both cases, the impedance spectra consist of two semicircles. However, they differ markedly from each other, depending on the presence of H_2. The impedance data can be fitted using an equivalent circuit comprising a combination of two resistor-constant phase elements in parallel with a geometrical capacitance C_{geo} (Figure 4a). $Z^*(\mathrm{RH})$ depends on the adjusted humidity, as discussed below. The constant phase element (CPE) is often used in equivalent circuit representations instead of pure capacitors and is attributed to surface inhomogeneity [23].

In the presence of hydrogen, the equivalent circuits, shown in Figure 4b, also contain the impedance $Z^*(\mathrm{RH})$ obtained at the same humidity without H_2. The capacitance values are calculated by converting the constant phase element to the capacitance, according to $C_{pseudo} = Y_0^{1/n} R^{(1-n)/n}$,[24] where C_{pseudo} is the resulting pseudocapacitance, Y_0 is the admittance, n is an empirical constant ranging from 0 to 1 and R is the resistance in parallel to CPE.

In order to relate the observed semicircles to corresponding elements of the Pt/TiO_2/Ti structure, one may use the complex relative permittivity, $\varepsilon(\omega)$, i.e. $\varepsilon(\omega) = \varepsilon'(\omega) - i\varepsilon''(\omega) = [Y(\omega)/i\omega C_0]$. Here, $\varepsilon'(\omega)$, $\varepsilon''(\omega)$, ω, C_0 and $Y(\omega)$ are the real and imaginary part of the relative permittivity, angular frequency, sample´s geometrical capacitance and admittance, respectively. Along with values of resistances, the geometric capacitance was obtained by fitting impedance data.

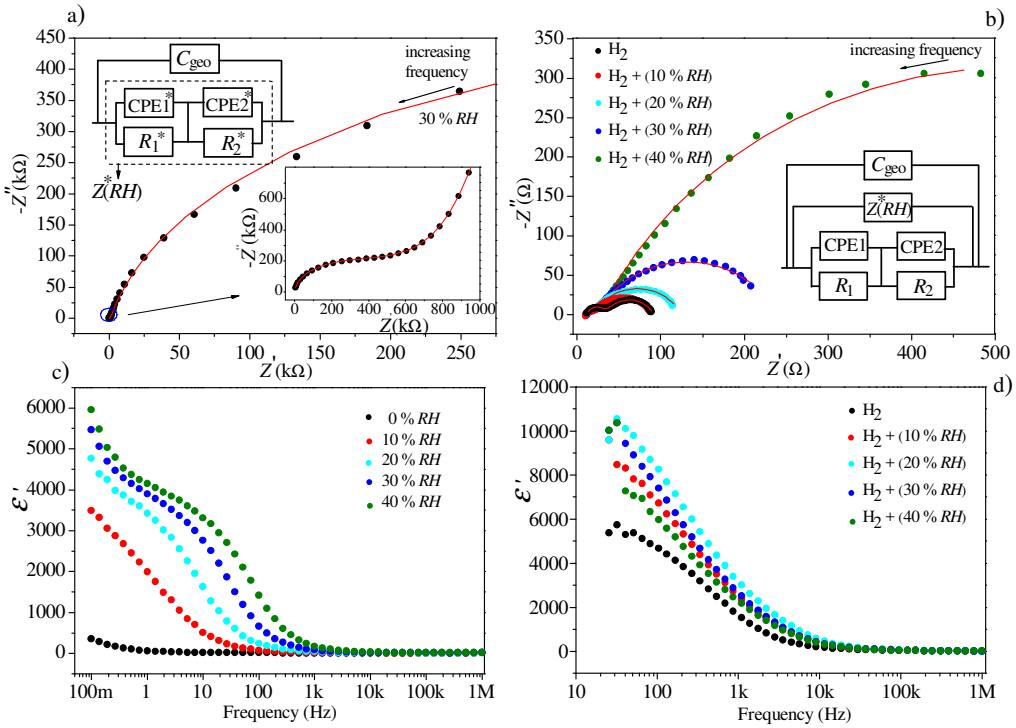

Figure 4. Impedance spectra (Nyquist plot, i.e., representation of the real and imaginary parts $Z'$and Z'', respectively, in the complex plane as a function of frequency) of Pt/TiO_2/Ti measured at different humidity **(a)** without H_2 and **(b)** with 2.1 vol% H_2 (dots). Fitted values are shown as red solid lines. Insets represent models of the equivalent circuits. R_1 (R_1*), R_2 (R_2*) and CPE (CPE*) represent the grain boundary resistance of TiO_2, the charge transfer resistance, and are the constant phase element with and without hydrogen. $Z^*(RH)$ denotes the impedance of the sample without hydrogen. The evolution of $\varepsilon'(\omega)$ of Pt/TiO_2/Ti with frequency is shown in **(c)** the absence and **(d)** the presence of hydrogen.

Figure 4 (c) and (d) show the evolution of $\varepsilon'(\omega)$ of Pt/TiO_2/Ti with humidity. It is clear that $\varepsilon'(\omega)$ is very high in low frequency regions for both cases, particularly in hydrogen. The high value at low frequencies may be associated with an electrode polarisation effect. The capacitance values of C_2 and C_2^*were found to increase with increasing RH in low frequency regions (see Table 1). They can be related to a double layer at Pt/TiO_2 contact. The much smaller values of C_1 and C_1^* in high frequency regions may reflect the electrical properties of grain boundaries of TiO_2. Correspondingly, we attribute R_1 and R_1^* to the resistance of grain boundaries of TiO_2 and R_2 and R_2^* to the charge transfer resistance with and without hydrogen, respectively. For humid air, the charge transfer resistance R_2^*

decreases very slowly from 15 MΩ to 1 MΩ, while the values of grain boundary resistance R_1^* are reduced by three orders of magnitude relative to the value in dry air (2.5 MΩ). The decrease in R_1^* and R_2^* is consistent with our conclusions from the *I-V*-characteristics from Figure 3, suggesting a decrease in oxygen acceptor states in the Pt/TiO_2/Ti system. In the presence of hydrogen, the resistance of the grain boundary is significantly smaller, and it is further decreased upon adding water vapour (RH = 10 %). For humidity above 10 %, it increases slowly up to 40 %. It was found that the sum of the grain boundary resistance and charge transfer resistance in H_2 shows a good correlation with the internal resistance calculated from the ratios V_{oc}/I_{sc} (compare Figure 5) and its reciprocals $(R_1+R_2)^{-1}$ follow the volcano-type feature of J_{sc}.

Table 1. Resistances and capacitances obtained by fitting impedance spectra with equivalent circuits.

RH (%)	R_1^*(Ω)	C_1^*(nF/cm^2)	R_2^*(Ω)	C_2^*(μF/cm^2)
Dry air	2.5×10^6	24	15×10^6	3.7
10	3.2×10^4	84	3.0×10^6	5.4
20	8.5×10^3	108	1.5×10^6	5.5
30	3.0×10^3	140	1.1×10^6	5.56
40	1.2×10^3	176	1.0×10^6	5.6
H_2 + (*RH* (%))	R_1(Ω)	C_1(nF/cm^2)	R_2(Ω)	C_2(μF/cm^2)
(2.1 vol % H_2)	21	98	62	8.22
(2.1 vol % H_2) + (10)	8	356	70	8.72
(2.1 vol % H_2) + (20)	9	382	104	9.12
(2.1 vol % H_2) + (30)	11	278	217	9.42
(2.1 vol % H_2) + (40)	14	164	986	10.1

We will now discuss the experimental findings in terms of chemical and transport reactions that occur at TiO_2 and Pt. Since the current (i.e., the flux of electrons through the sample) is constant as long as steady-state gas fluxes of the incoming reactants H_2 and O_2 are maintained experimentally and the reaction product H_2O is constantly removed from the sample by the air flow, we must consider stationary conditions for these reactions.

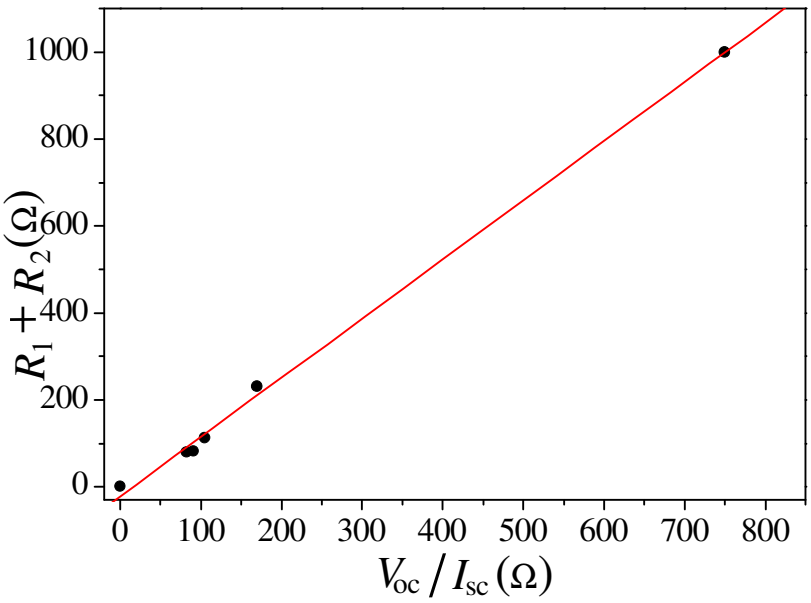

Figure 5. Correlation between the values of internal resistance V_{oc}/I_{sc} of Pt/TiO_2/Ti cells calculated from the *I-V* curves and the sum of the grain boundary resistance and charge transfer resistance evaluated from impedance spectra.

The suggested reactions that explain emf formation under steady-state conditions and the observed electron flow direction from the titanium to the platinum electrode are given in the scheme 1, applied for the short circuit condition ($V = 0$) in dry air.

We adopt the Kröger-Vink notation for a straightforward representation of sites and charges with respect to the regular charge at the corresponding lattice site (sites denoted by subscripts, charged species by superscripts: $^{\times}$= neutral, $^{\bullet}$ = positive, $^{\prime}$ = negative). We assume an electrostatically neutral TiO_2(110) surface for the discussion, since a previous study on the structure of the titanium oxide layer, prepared with our technique, has revealed that rutile is the predominant phase in our system [20]. Scheme 1 comprises a series of surface reactions which have been studied by many groups over recent decades in order to gain insight into fundamental interactions of TiO_2, Pt, and Pt/TiO_2 with hydrogen, oxygen, and water.

Scheme 1. Surface reactions and charge transfer

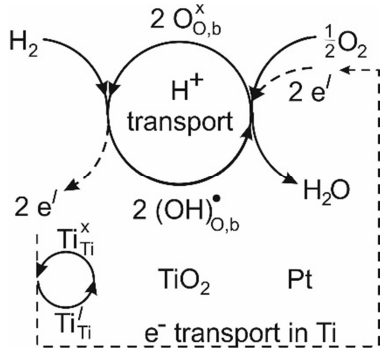

The interaction of TiO_2(110) with atomic hydrogen has been previously studied with He scattering. Kunat et al. confirmed the existence of a (1×1) adlayer of H atoms [25]. An earlier investigation by Göpel et al. demonstrated the role of surface defects in the interaction with molecular H_2 [26]. The reducibility of metal oxides by hydrogen is well known and commonly associated with the formation of oxygen vacancies as a result of water formation at elevated temperature [27]. The reaction can be written as shown in scheme 2.

Scheme 2. Hydrogen interaction with lattice oxygen

$$H_2 + O_O^\times \rightarrow H_2O + V_O^{\bullet\bullet} + 2\ e'$$

The interaction of water with surface oxygen vacancies has attracted great interest, especially for TiO_2, because of its importance in many technological applications. Scanning tunnelling microscopy, which indicates adsorbed H atoms as small protrusions in the STM images, and theoretical DFT calculations have confirmed the dissociation of water onto defective TiO_2 surfaces, [28,29] thereby forming two bridging oxygen hydroxyls. Taking into account the predominance of bridge-bonded oxygen vacancies on TiO_2(110) (frequently called BBO_v, here notated as $V^{\bullet\bullet}_{O,b}$ for consistency), such a reaction can be written as scheme 3.

Scheme 3. Dissociation of water on surface

$$H_2O + V_{O,b}^{\bullet\bullet} + O_{O,b}^{\times} \rightarrow 2\,(OH)_{O,b}^{\bullet}$$

Although hydroxyl groups at bridging and terminal sites (coordinated on metal ions of the lattice) have been considered to explain acidic and basic properties for many oxides (i.e., H^+ donating and accepting properties in water), [30] terminal $(OH)_{O,t}^{\times}$ is apparently not formed during water adsorption onto defective TiO_2(110) under ultra-high vacuum conditions. The demonstration of two inequivalent OH groups on TiO_2(110) is related to the observed difference in diffusion rates [9].

Scheme 1 suggests the formation of two charged surface hydroxyl groups at O bridging surface sites during the interaction between hydrogen and the TiO_2 film at room temperature. Because of electrostatic neutrality, the reaction must release two electrons per molecule into TiO_2 in accordance with the increased conductivity of Pt/TiO_2/Ti (Figure 1, black curve). Formally, this reaction step corresponds to a subsequent reaction of (2) and (3) if $O_O^{\times}$ is assigned to a bridging site. Moreover, hydrogen may also be absorbed as an atom, formed by dissociative adsorption at Pt sites, and transferred to the TiO_2 surface by spill-over, as suggested by Ref. [6,31].

Surface diffusion of protons occurs until they react with oxygen and electrons at Pt sites to form water. The diffusion of hydrogen is an intrinsic property of TiO_2 and has been recently clarified with STM. A pre-factor of $10^{7.3\pm0.4}$ and an activation energy of 0.74 ± 0.3 eV have been determined from Arrhenius plots, based on temperature-dependent STM experiments on TiO_2(110) [9].

The transport of electrons through the lattice is described as hopping process involving Ti^{4+} ($Ti_{Ti}^{\times}$) and Ti^{3+} ions (Ti_{Ti}') in accordance with experimental studies which confirm the strong electron-phonon coupling in TiO_2 [32]. Since the current flows from Ti to Pt in the outer circuit at $V = 0$, there is no net electron transport

internally over the depletion zone at the Pt/TiO_2 interface; however, actual current exchange rates at the interface are unknown.

The emf is generated due to a difference in the hydrogen partial pressures at the Pt/TiO_2 interface and on distant TiO_2 surface sites, which creates a difference in chemical potential. At Pt sites, the oxidation of hydrogen reduces the local hydrogen partial pressure when compared with the value over TiO_2 surface sites. It is evident that the larger electron density in the TiO_2, proposed by reaction (1), explains the large current in the reversed bias regime of Figure 1 (black curve), found in dry air with 2.1 vol% H_2.

An obvious effect of the humidity on the short circuit current density (i.e., at $V = 0$) is the volcano-type behaviour of J_{sc}, with a maximum around RH = 10 %, distinctly different from the gradual decrease in current density in the reversed bias regime and turnover numbers for H_2-to-H_2O oxidation at the platinum electrode.

To explain this feature of Pt/TiO_2/Ti, we first recapitulate the influence of humidity on TiO_2 in the absence of hydrogen, which is associated with a "quasi-donor" effect (compare forward bias voltage regime, Figure 3).

Water can displace adsorbed oxygen from surface sites. Let us assume that O atoms have captured vacant sites above the five-fold coordinated Ti ions of the surface, denoted here as terminal $O'_{O,t}$ which have trapped negative charge. Then one can formulate the hydroxylation of the TiO_2 surface with pre-adsorbed oxygen as shown in scheme 4.

Scheme 4. Reaction of water with surface oxygen

$$H_2O + O'_{O,t} \rightarrow e' + (OH)^{\times}_{O,t} + (OH)^{\times}_{O,b}$$

Here we mention atomic oxygen adsorbates, $O'_{O,t}$, because of the presence of platinum and a spillover of O from Pt sites. It is evident from the Schottky barrier heights and ideality factors that even at RH = 40 % a major portion of the TiO_2

surface is occupied with negatively charged oxygen. Reaction (4) suggests that bridging and terminal hydroxyl groups are present to some extent at the TiO_2 surface at equal concentrations.

The presence of bridging hydroxyl at the TiO_2 surface opens another reaction channel for molecular oxygen adsorption, known as the electron "scavenging" process. The process is observed during photocatalysis with TiO_2, in which O_2 scavenges photo-induced electrons [33]. As proposed by Henderson *et al.*[17] the process in scheme 5 converts bridging OH groups to terminal OH groups, $(OH)^{\times}_{O,t}$, thereby replenishing the bridging site with oxygen [34] Reaction (4) requires vacant terminal sites on top of fivefold coordinated surface Ti ions. The occurrence of reaction (5) would reduce the blocking effect of water with respect to the interaction of hydrogen with $O^{\times}_{O,b}$ (compare scheme 1).

Scheme 5. Conversion of surface hydroxyls by molecular oxygen

$$(OH)^{\times}_{O,b} + \frac{1}{2}O_2 \rightarrow (OH)^{\times}_{O,t} + O^{\times}_{O,b}$$

An investigation into the reaction between O_2 and bridging hydroxyls at TiO_2(110) at different coverages of water, performed using temperature programme desorption (TPD) and vibrational electron energy loss spectroscopy (EELS), suggests that a layer of water blocks the access of O_2 to the TiO_2 surface [17]. As a consequence, the conversion of $(OH)^{\times}_{O,b}$ to terminal hydroxyls is hindered and the rate of hydrogen reaction with $O^{\times}_{O,b}$ should be smaller than in dry air. Such a process can be regarded as an acceptor-type effect of water vapour in the presence of hydrogen. This is in accordance with the observed reduction of the current in the reversed bias voltage regime of Pt/TiO_2/Ti (compare Figure 1). There is another feature that is evidenced from the *I-V* characteristics in that voltage regime: the beginning of a saturation of the current for voltages below approximately -0.5 V at RH $\geq$ 10 %.

At RH = 40 %, it is obvious that a further increase in voltage (in terms of absolute values) does not significantly increase the current. The differential conductance dI/dV of the TiO_2 approaches zero at RH = 40 %. This is in contrast to the *I-V* characteristics of Pt/TiO_2/Ti in dry air with 2.1 vol% H_2. The fact that the current approaches some sort of saturation is consistent with a limited rate of hydrogen adsorption on $O^{\times}_{O,b}$ and a corresponding limited rate by which electrons are released to TiO_2 from this reaction.

To explain the observed maximum of J_{sc} between RH = 0 to 20 %, we will inspect the dependency of grain boundary and the charge-transfer resistance, since $(R_1+R_2)^{-1}$ (see Table 1) corresponds in a good approximation to the volcano-type function of J_{sc}(RH). However, only the grain boundary resistance decreases as J_{sc} increases. Therefore, it seems that the increase in J_{sc} is much better correlated with the change in grain boundary resistance, which is related to electron transport. Recent experimental and theoretical investigations on the interaction of water with OH groups on TiO_2 have shown an unoccupied state of 2.4 eV above the Fermi level [35,36]. Based on the calculations of density functional theory, the state is attributed to a partially hydrated "wet-electron" state localized on the surface. The extremely strong coupling between wet-electron states [37] may provide injection channels along the oxide surface which can therefore enhance electron transport through the TiO_2 porous structure to the Ti contact, described her as occurring via electron hopping over Ti^{4+} lattice ions. The wet-electron state requires cooperative interaction between H_2O and OH on TiO_2, and its maximum intensity depends on a ratio between a certain amount of H_2O and H [35]. The relevant structure for maximum intensity of wet-electron states in our experiment may be formed at 2.1 vol % H_2 with additional 10 % *RH*, which may be responsible for the increase in J_{sc} from 8.2 mA/cm^2 in dry air to 9.4 mA/cm^2.

Upon additional exposure to values of RH $\geq$ 20 %, the decrease in J_{sc} may be associated with the blocking effect of water as the rate of reaction (3) becomes

smaller. The decreased rate concerns all of the coupled reactions, including the release of electrons from the hydrogen interaction with bridging oxygen.

A final comment must be made about the increasing values of the open circuit voltage V_{oc} with increasing RH. According to our model of emf generation in Pt/TiO_2/Ti, V_{oc} is related to the chemical potential difference between both sites and is proportional to $ln\left[p_{TiO_2}(H_2)/p_{Pt}(H_2)\right]$. Because of the adverse influence of water vapour on the catalytic turnover of H_2-to-H_2O, as found in our microcalorimetry experiments, an increase in the hydrogen partial pressure over Pt sites is expected. This also implies a decrease in V_{oc}. However, the experimental values of V_{oc} run contrary to this expectation. The first explanation that comes to mind is based on the increased permittivity found in the low frequency region of impedance spectra. This reflects the formation of a double layer at the Pt/TiO_2 interface that causes a voltage drop, V_{drop}. As is already known, V_{oc} can be considered as an external counter voltage, V_{ext}, which is applied to compensate for the emf. If a double layer forms, V_{ext} does not correspond to the true open circuit voltage V_{oc}^{true}, since V_{ext} includes V_{drop}, i.e., $V_{ext} = V_{oc}^{true} + V_{drop}$. Thus, as V_{drop} increases with increasing RH, larger values of V_{ext} are required to compensate for emf, which may be a reasonable explanation for the observed result for V_{oc}.

2.4 Conclusions

We studied the humidity influence on Pt/TiO_2/Ti emf cells, operated to 2.1 vol% hydrogen in air, using dc and ac techniques. We demonstrated that adding water vapour to the air causes the short circuit current to rise around RH 10 %, while further increases in humidity lead to decreases in short circuit current. The open-circuit voltage was observed to always increase for all adjusted humidity values. The results of our investigations indicate the predominant role of TiO_2-related surface processes that determine the *I-V* characteristics and impedance of Pt/TiO_2/Ti. We have shown that the sum of grain boundary and charge transfer resistance, determined from the high- and low-frequency regime of the impedance

spectra, is correlated with the internal resistance of the cell and that the volcano-type behaviour of J_{sc} when varying the humidity follows the change in both resistances. Our results may have implications for the potential application of $Pt/TiO_2/Ti$ structures such as single-chamber fuel cells and hydrogen gas sensors in humid air.

2.5 References

[1] Bagotsky, V. S., *Fuel cells: problems and solutions*; John Wiley & Sons, 2nd ed., **2011**

[2] Napporn, T. W.; Kuhn, M. Single-chamber fuel cells. In: *Fuel cell science and engineering: materials, processes, systems, Vol. 1*; D. Stolten and B. Emonts (Eds.), Wiley VCH, **2012**.

[3] Jiang, S. P.; Shen, P. K. (Eds.) *Nanostructured and Advanced Materials for Fuel Cells*; CRC Press, Taylor & Francis, **2014**.

[4] Najafpour, G. *Biochemical Engineering and Biotechnology*; Elsevier, **2015**, p. 528.

[5] Schierbaum, K.; El Achhab M. Generation of an electromotive force by hydrogen-to-water oxidation with Pt-coated oxidized titanium foils. *Phys. Status Solidi A* **2011**, .DOI 10.1002/pssa.201127400F

[6] Karpov, E. G.; Hashemian, M. A.; Dasari, S. K. Chemistry-Driven Signal Transduction in a Mesoporous Pt/TiO_2 System. *J. Phys. Chem. C* **2013**, *117*, 15632-15638.

[7] Hashemian, M. A.; Palacios, E.; Nedrygailov, I. I.; Diesing, D.; Karpov, E. G. Thermal Properties of the Stationary Current in Mesoporous Pt/TiO_2Structures in an Oxyhydrogen Atmosphere. *ACS Appl. Mater. Interfaces* **2013**, *5*, 12375-12379.

[8] Cakabay, Ö.; El Achhab, M.; Schierbaum, K. Thermal properties of solid-state Pt/TiO_2/Ti emf cells studied by microcalorimetry. *Appl. Phys. A* **2015**, *118*, 1127-1132.

[9] Zhang, Z.; Bondarchuk, O.; Kay, B. D.; White, J. M.; Dohnálek, Z. Imaging Water Dissociation on TiO_2(110): Evidence for Inequivalent Geminate OH Groups. *J. Phys. Chem. B* **2006**, *110*, 21840-21845.

[10] Wendt, S.; Matthiesen, J.; Schaub, R.; Vestergaard, E. K.; Lægsgaard, E.; Besenbacher, F.; Hammer, B. Formation and splitting of paired hydroxyl groups on reduced TiO2(110). *Phys. Rev. Lett.* **2006**, *96*, 066107.

[11] Bikondoa, O.; Pang, C. L.; Ithnin, R.; Muryn, C. A., Onishi, H.; Thornton, G. Direct visualization of defect-mediated dissociation of water on TiO_2 (110). *Nature Materials* **2006**, *5*, 189-192.

[12] Ketteler, G.; Yamamoto, S.; Bluhm, H.; Andersson, K.; Starr, D. E.; Ogletree, D. F.; Ogasawara, H.; Nilsson, A.; Salmeron, M. The nature of water nucleation sites on TiO_2 (110) surfaces revealed by ambient pressure X-ray photoelectron spectroscopy. *J. Phys. Chem. C* **2007**, *111*, 8278-8282.

[13] Mao, X.; Lang, X.; Wang, Z.; Hao, Q.; Wen, B.; Ren, Z.; Dai, D.; Zhou, C.; Liu, L.-M.; Yang, X. Band-Gap States of TiO_2(110): Major Contribution from Surface Defects. *J. Phys. Chem. Lett.* **2013**, *4*, 3839-3844.

[14] Valentin, C. D.; Tilocca, A.; Selloni, A.; Beck, T. J.; Klust, A.; Batzill, M., Losovyj, Y.; Diebold, U. Adsorption of water on reconstructed rutile TiO_2(011)-(2 x 1): Ti=O double bonds and surface reactivity. *J. Am. Chem. Soc.* **2005**, *127*, 9895-9903.

[15] Du, Y.; Deskins, N. A.; Zhang, Z.; Dohnalek, Z.; Dupuis, M.; Lyubinetsky, I. Two Pathways for Water Interaction with Oxygen Adatoms on TiO_2. *J. Phys. Chem. C* **2010**, *114*, 17080–17084.

[16] Zhang, Z.; Cao, K.; Yates, J. T. Jr. Defect-Electron Spreading on the TiO_2(110) Semiconductor Surface by Water Adsorption. *J. Phys. Chem. Lett.* **2013**, *4*, 674-679.

[17] Henderson, M. A., Epling, W. S.; Peden, C. H. F.; Perkins, C. L. Insights into Photoexcited Electron Scavenging Processes on TiO_2 Obtained from

Studies of the Reaction of O_2 with OH Groups Adsorbed at Electronic Defects on TiO_2(110). *J. Phys. Chem. B* **2003**, *107*, 534-545.

[18] Masel R. I. *Principles of Adsorption and Reaction on Solid Surfaces*; John Wiley & Sons, **1996**, p438.

[19] Gorodetskii, V. V.; Sametova, A. A.; Matveev, A. V.; Tapilin, V. M. From single crystals to supported nanoparticles in experimental and theoretical studies of H_2 oxidation over platinum metals (Pt, Pd): Intermediates, surface waves and spillover. *Catalysis Today* **2009**, *144*, 219-234.

[20] El Achhab, M.; Erbe, A.; Koschek, G.; Hamouich, R.; Schierbaum, K. A microstructural study of the structure of plasma electrolytically oxidized titanium foils. *Appl. Phys. A* **2014**, *116*, 2039-2044.

[21] Henderson, M. A.; Epling, W. S.; Perkins, C. L.; Peden, C. H. F.; Diebold, U. Interaction of Molecular Oxygen with the Vacuum-Annealed TiO_2(110) Surface: Molecular and Dissociative Channels. *J. Phys. Chem. B* **1999,** *103*, 5,328-5,337

[22] Kim, C. K.; Lee, J. H.; Choi, S. M.; Noh, I. H.; Kim, H. R.; Cho, N. I.; Hong, C.; Jang, G. E. Pd- and Pt-SiC Schottky diodes for detection of H_2 and CH_4 at high temperature. *Sensors and Actuators B* **2001**, *77*, 455-462.

[23] Brug, G.J., van den Eeden A.L.G.; Sluyters-Rehbach M.; Sluyters J.H. The analysis of electrode impedances complicated by the presence of a constant phase element. *J. Electroanal. Chem.* **1984**, 176, 275-295.

[24] Orazema, M. E.; Frateur, I.; Tribollet, B.; Vivier, V.; Marcelin, S.; Pébère, N.; Bunge, A. L.; White, E. A.; Riemer, D. P.; Musiani, M. Dielectric Properties of Materials showing Constant-Phase Element (CPE) Impedance Response. *J. Electrochem. Soc.* **2013**, *160*, C215-C225.

[25] Kunat, M.; Burghaus, U.; Wöll, C. The adsorption of hydrogen on the rutile TiO_2(110) surface. *Phys. Chem. Chem. Phys*. **2004**, *6*, 4203-4207.

[26] Göpel, W.; Rocker, G.; Feierabend, R. Intrinsic defects of TiO_2(110): Interaction with chemisorbed O_2, H_2, CO, and CO_2. *Phys. Rev. B* **1983**, *28*, 3427-3438.

[27] Kogler, M.; Köck, E.-M.; Bielz, T.; Pfaller, K.; Klötzer, B.; Schmidmair, D.; Perfler, L. Penner, S. Hydrogen Surface Reactions and Adsorption Studied on Y_2O_3, YSZ, and ZrO_2. *J. Phys. Chem. C* **2014**, *118*, 8435-8444.

[28] Schaub, R.; Thostrup, P.; Lopez, N.; Lægsgaard, E.; Stensgaard, I.; Norskov, K. K.; Besenbacher, F. Oxygen Vacancies as Active Sites for Water Dissociation on Rutile TiO_2(110). *Phys. Rev. Lett.* **2001**, *87*, 266104.

[29] Brookes, I. M.; Muryn, C. A.; Thornton, G. Imaging Water Dissociation on TiO_2(110). *Phys. Rev. Lett.* **2001**, *87*, 266103.

[30] Tamura, H., Mita, K.; Tanaka, A. Ito, M. Mechanism of Hydroxylation of Metal Oxide Surfaces. *J. Colloid and Interf. Sci.* **2001**, *243*, 202-207.

[31] Prins, R. Hydrogen Spillover. Facts and Fiction. *Chem. Rev.* **2012**, *112*, 2714-2738.

[32] Hendry, E.; Wang, F.; Shan, J.; Heinz, T. F.; Bonn, M. Electron transport in TiO_2 probed by THz time-domain spectroscopy. *Phys. Rev. B* **2004**, 69, 081101.

[33] Linsebigler, A.; Lu, G.; Yates, J. T. Photocatalysis on TiO_2 Surfaces: Principles, Mechanisms, and Selected Results. *Chem. Rev.* **1995**, *95*, 735-738.

[34] Petrik, N. G.; Zhang, Z.; Du, Y.; Dohnálek, Z.; Lyubinetsky, I.; Kimmel, G. A. Chemical Reactivity of Reduced TiO_2(110): The Dominant Role of Surface Defects in Oxygen Chemisorption. *J. Phys. Chem. C* **2009**, *113*, 12407-12411.

[35] Onda, K.; Li, B.; Zhao, J.; Jordan, K. D.; Yang, J.; Petek, H. Wet Electrons at the H_2O/TiO_2(110) Surface. *Science* **2005**, *308*, 1154-1158.

[36] Zhao, J.; Li, B.; Onda, K.; Feng, M.; Petek, H. Solvated Electrons on Metal Oxide Surfaces. *Chem. Rev*. **2006**, *106*, 4402-4427.

[37] Fischer, S. A.; Duncan, W. R.; Prezhdo, O. V. Ab Initio Nonadiabatic Molecular Dynamics of Wet-Electrons on the TiO_2 Surface. *J. Am. Chem. Soc*. **2009**, *131*, 15483-15491.

Journal: The Journal of Physical Chemistry C

Impact Factor: 4.509

Own contribution: 75%

1. Author

Chapter 3

Thermal activation of $Pt/TiO_2/Ti$ emf cell

We investigated the effects of thermal activation of $Pt/TiO_2/Ti$ electromotive force (emf) cells which operate with hydrogen-in-air mixtures through a short heating process called "flashing". Samples are prepared using a plasma electrolytic oxidation process of Ti foils and deposition of Pt paste, followed by thermal treatment in air. The samples then produce an electromotive force when they are exposed to hydrogen-in-air mixtures. However, samples stored in ambient air undergo an aging process that results in them producing only small emfs and current densities in hydrogen-in-air mixtures. After preparation, flashing in air prior to operation restores the initial active state. We find significant differences in the magnitude of current densities (J_{sc}) and response times before and after flashing. The current density (J_{sc}) of untreated $Pt/TiO_2/Ti$ samples shows a slow increase with hydrogen exposure time, whereas it rises rapidly after flashing and converges to a constant value of 6.1 mA/cm^2 which is approximately 400 times larger than the current density of an untreated sample. Flashed and untreated TiO_2 samples show identical microstructures in images from scanning electron microscopy and atomic force microscopy. Raman spectroscopy indicates no change in the relative amounts of crystalline anatase and rutile phases, which constitute the TiO_2. X-ray photoelectron spectroscopy confirms that no titanium suboxide phases are formed by flashing. However, electrochemical impedance spectroscopy shows a significantly reduced internal resistance of samples after flashing, which is in accordance with the large and constant values of current densities after flashing. The results are interpreted as follows. As a consequence of aging, a large number of acceptor-like oxygen surface states are formed that reduce electron transport, particularly at grain boundaries of TiO_2 films. Flashing removes the majority of these states and thus increases electron conductivity.

3.1 Introduction

Recent studies addressing the generation of an electromotive force (emf) over platinum-coated plasma electrolytically oxidized titanium foils ($Pt/TiO_2/Ti$) in hydrogen-in-air mixtures at room temperature have been reported [1-4]. If samples are not used immediately after their preparation in which the final step includes a thermal treatment, and are left unused, then a short thermal treatment, typically at 700°C for 30 s, must be applied prior to emf generation. An obvious explanation for the aging of $Pt/TiO_2/Ti$ cells in ambient air would be that gases such as oxygen, water vapor, and carbon dioxide are adsorbed. A recent study on the effect of water vapor on emf generation confirms a substantial influence of water [5].

It is well known that oxygen, during its adsorption on a TiO_2 surface, traps electrons originating from defects, doping or photoexcitation [6,7]. As a result, a large number of adsorbed O_2^-, O_2^{2-} and O_4^{2-} species are formed [6-9]. The O_2^- species has been reported to be the most stable oxygen species on the TiO_2 surface,[10,11] and it desorbs as O_2 at $T > 410$ K, as shown by Henderson et al. [8] with thermal desorption spectroscopy (TDS).

Polycrystalline thin TiO_2 films show strongly decreased conductivity owing to oxygen-induced trap states located at the surface and the interface of grain boundaries [12]. $Pt/TiO_2/Ti$ show *I-V* characteristics upon exposure to oxygen in ultra-high vacuum or air in ambient conditions, which corresponds almost to an isolator [2,5]. This effect is associated with a large density of states at the Pt/TiO_2 interface that pins the band edges relative to the Fermi level.

The adsorption of CO_2 on the TiO_2 surface has attracted great interest due to the photocatalytic reduction of CO_2. It is known that CO_2 is an inert molecule with a positive electron affinity of 0.6±0.2 eV [13]. Further, its lowest unoccupied molecular orbital (LUMO) is very high [14], indicating that the electron transfer from TiO_2 to CO_2 to form CO_2^- is energetically unfavorable [15]. Henderson [16] investigated CO_2 adsorption on the rutile TiO_2 (110) surface using the techniques

of temperature programmed desorption (TPD), static secondary ion mass spectrometry (SSIMS), and high resolution electron energy loss spectrometry (HREELS). It was shown that CO_2 weakly adsorbs on the surface and binds preferentially to the oxygen vacancy sites. Furthermore, the pre-adsorbed H_2O on the surface blocks CO_2 adsorption. A TPD experiment, giving a zero-coverage CO_2 binding energy of 0.56 eV, confirms the weak interaction between CO_2 molecules and the rutile TiO_2 (110) surface [17]. It should be noted that CO_2 binding energy on the vacancy site is lower than that of the H_2O binding energy (0.64 eV) and O_2 binding energy (2.78 eV) [18]. Based on these results, the influence of CO_2 adsorption on the aging may be expected to be less evident in the presence of O_2 or H_2O.

In this paper we used scanning electron and atomic force microscopy, Raman and x-ray photoelectron spectroscopy, and electrochemical impedance spectroscopy to study the effects of flashing on Pt/TiO_2/Ti samples.

3.2 Experimental

Titanium foils (10×10 mm^2, 125 µm thick) were plasma electrolytically oxidized to yield a porous titanium dioxide structure. The oxidation was performed in magnetically stirred 14 M sulfuric acid in water-jacketed double-walled glass (Neubert-Glas, volume 250 ml) with an inlet and an outlet, connected to a refrigerated circulator (FP50, Julabo). Thus, the electrolyte temperature remained constant during preparation. A graphite rod was used as cathode. The oxidation voltage was increased stepwise to a final value of 150 V, while the current was kept constant at 200 mA. The recipe is given in [19]. The oxidized Ti foil was subsequently washed in deionized water and then dried at 100°C for 1 min. For the top electrode, a platinum paste (Chempur) was applied to the surface of the titanium dioxide sample. The area of Pt on theTiO_2-samples was 5×5 mm^2. The sample was then heated in air at 700°C for 30 s to remove the organic compounds of the paste before being stored for a period of one week in ambient air.

Prior to the experiment, the sample was purged for 3 h in pure air that had a flow of 100 ml/min. This was done to remove residual humidity from the internal walls of the test chamber and sample. The sample was then exposed to a 3.5 vol% hydrogen-in-air mixture. The transient currents generated were determined at room temperature in a gas-flow apparatus described in detail in ref. [4,5].

Electrochemical impedance spectra (EIS) were determined using an Autolab instrument (PGSTAT302N, Metrohm) combined with a FRA32M module in a frequency range between 1 MHz and 15 Hz. The amplitude of the AC signal and the DC bias voltage were 20 mV and zero, respectively.

The surface morphology of the TiO_2 films was determined by scanning electron microscopy (SEM) with a Supra 40 VP and a field emission electron source (Zeiss) and by atomic force microscopy (Bruker Dimension Icon). The Raman spectra were collected with a confocal Raman microscope (InVia, Renishaw) with HeNe laser radiation (532 nm). X-ray photoelectron spectra (XPS) were recorded with Al Kα radiation and a hemispherical analyzer (VersaProbe II, Ulvac-Phi).

3.3 Results and Discussion

3.3.1 Structural Characterization

Scanning electron microscopy (SEM) of uncoated samples confirms that the titanium oxide films possess a porous structure with pores in the micron and sub-micron range (Figure 1a). The atomic force microscopy (AFM) image in Figure 1b depicts an uneven sample surface with depression areas at different depths. The observation of spherically shaped oxide particles (one is marked with dashed circle in Figure 1a with a diameter of 120 nm) indicates the occurrence of high local temperatures during plasma electrolytic oxidation. The thickness of the titanium oxide layer is about 15 µm, as determined from microscopic images of cross sections of the sample.

Raman spectra of titanium oxide-covered foils were recorded after storing the samples for a couple of days in ambient air. A typical spectrum is shown in Figure

1c (black curve). It confirms the presence of anatase and rutile in accordance with earlier investigations [19]. The spectrum and the relative portions of these TiO_2 phases remain unchanged after heat treatment at 700°C for 30 s in air (red curve), which corresponds to the flashing procedure of the $Pt/TiO_2/Ti$ samples. It should be noted that both phases are stable at room temperature. The thermally-induced phase transformation from anatase to rutile, thermodynamically favored for the crystallite sizes in our samples, requires prolonged heating times and does not proceed to a significant extent within the 30 s flash at 700°C.

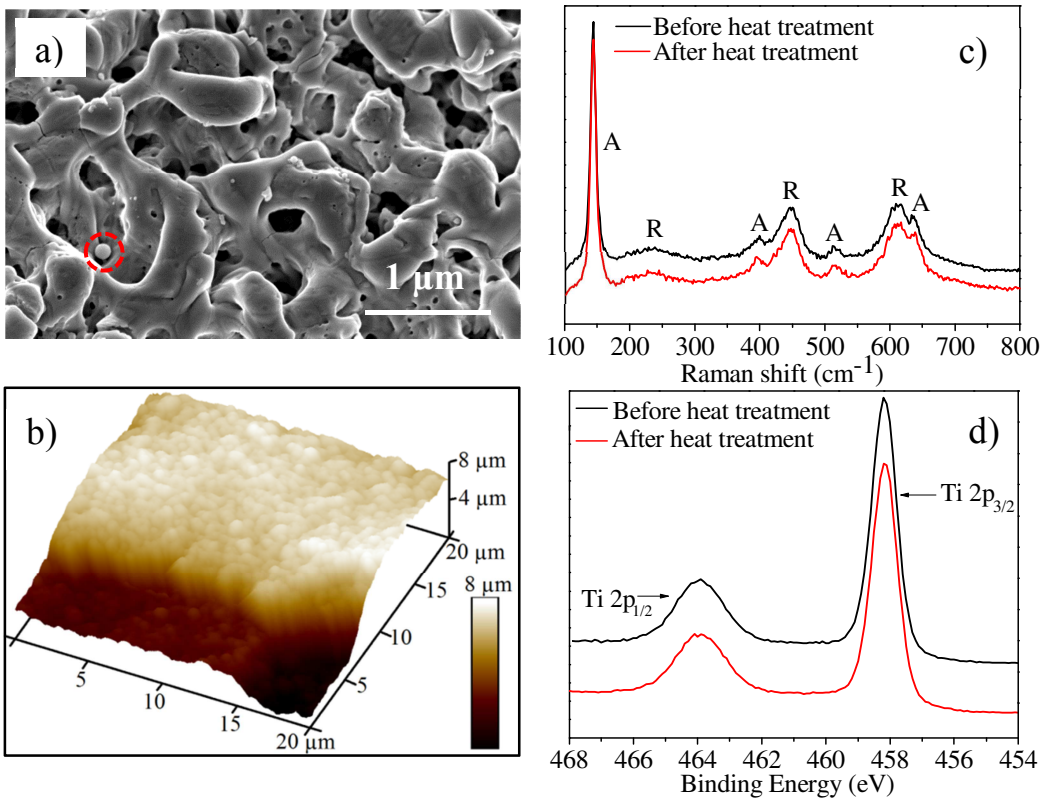

Figure 1 (a). SEM image and **(b)** AFM image of the surface of the uncoated TiO_2/Ti sample; **c)** Raman spectra before and after flashing of the sample in air; **d)** XPS Ti 2p core level spectra before and after flashing.

Figure 1d shows the XPS spectra of the Ti 2p core levels. The spin-orbit split Ti $2p_{1/2}$ and Ti $2p_{3/2}$ peaks centered at 464.0 eV and 458.3 eV, respectively, are symmetric and are associated with the +4 oxidation state of titanium in TiO_2 [20]. There are no visible changes in the XPS spectra before and after heat treatment in

terms of Ti $2p_{1/2}$ and Ti $2p_{3/2}$ binding energies and Ti $2p_{3/2}$-to-O1s intensity ratios. We conclude from these findings that no suboxides of titanium are formed during flashing.

3.3.2 Current Transients during EMF Generation

Figure 2 shows the transient response time of a current and an aged sample during hydrogen-air exposure before and after flashing. The current density (J_{sc}) rises very slowly from 0.4 nA/cm^2 considered the zero value under no bias to a value of 13 µA/cm^2 after an H_2 exposure time t = 60 min. For the heat treatment, the sample is then taken out of the measurement chamber, flashed at 700°C for 30 s, re-mounted immediately in the chamber and exposed to the same hydrogen-in-air mixture.

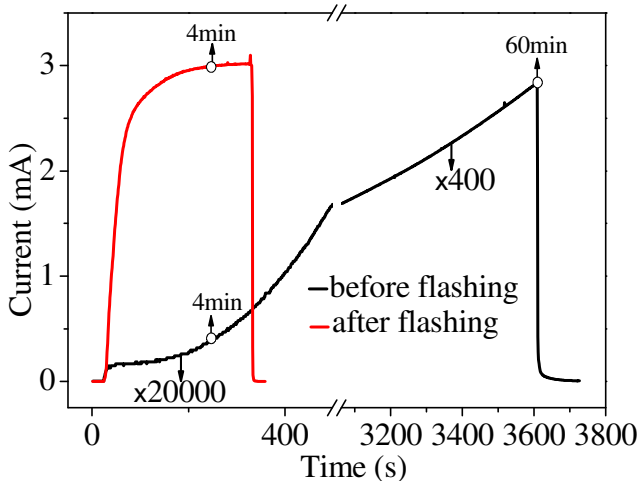

Figure 2. The generated transient current of a Pt/TiO_2/Ti sample with H_2 exposure before (black) and after (red) flashing. Electrochemical impedance spectra were recorded at 4 min for the flashed sample and at different exposure times ranging from 2 min to 60 min for the sample before flashing (marked positions indicate some selected times).

After heat treatment, the J_{sc} rises quickly, as can be seen in Figure 2b. For example, it reaches approximately 1 mA at a H_2 exposure time of $t \approx 10$ s, and at $t \approx 4$ min it becomes constant at a current density of 6.1 mA/cm^2. This is over 4 orders of magnitude higher than the value of the J_{sc} obtained at t = 4 min before flashing. The observed constant values are still over 400 times greater than the values of the untreated sample at t = 60 min.

Based on the results of numerous prepared samples, a flashing temperature between 650 and 700°C appears to represent the best choice for generating such constant and high values of current densities.

Figure 3a displays impedance spectra (Nyquist plots) in a log-log representation between 15 Hz and 1 MHz. The upper spectrum indicates the aged sample. It corresponds to a single semicircle in a linear plot Z'-*versus*-Z''. Further spectra were recorded at different H_2 exposure times; namely at t = 2, t = 4, t = 10 min, and after 10 min in 10 min steps until t = 60 min (compare Figure 2). In linear representations two semicircles are found. The impedance spectrum after flashing (brownish dots) demonstrates a substantial decrease in the real and imaginary parts Z' and Z'', respectively, with respect to the aged sample. The impedance spectrum after exposure to hydrogen is shown by the dark green dots at t = 4 min. Likewise, significant changes in phase angles are observed in phase angle versus frequency diagrams (Bode plots), as depicted in Figure 3b. With increasing times the initially predominant capacitive behavior of Pt/TiO_2/Ti, which shows a phase angle near 90° in the entire frequency range, gradually converts into a resistive behavior at low frequencies, although remains capacitor-like at high frequencies. The flashed Pt/TiO_2/Ti sample shows an almost resistive behavior at high frequencies; only the low frequency part behaves capacitively. In hydrogen, the most striking effect concerns the low frequency part as it shows a complete conversion from capacitor-like to resistor-like behavior.

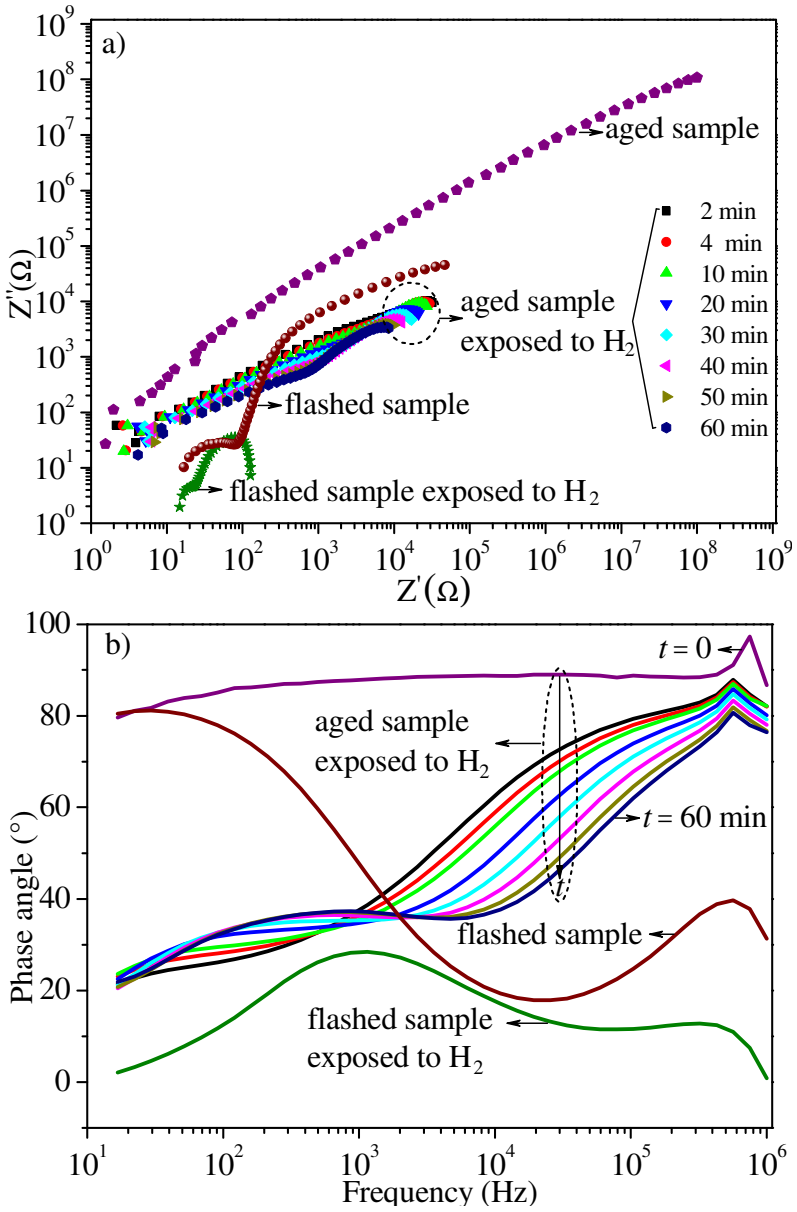

Figure 3 a). Impedance spectra of $Pt/TiO_2/Ti$ measured in a log-log representation before and after heat treatment and for H_2 exposure for different times. **b)** Corresponding phase angle *versus* frequency plots of $Pt/TiO_2/Ti$.

The impedance data is fitted by an equivalent circuit which consists of a combination of two resistor-constant phase elements in parallel with a geometrical capacitance [5] indicating a TiO_2-related grain boundary contribution at high frequency and a low frequency contribution that is associated with the Pt/TiO_2 interface. Hence, the internal resistance (R_{int}) of the $Pt/TiO_2/Ti$ emf cell comprises

two resistances (R_1 and R_2) that represent the grain boundary resistance of TiO_2 and the charge transfer resistance at Pt/TiO_2, respectively. The single semicircle, observed at the aged sample, indicates that R_1 and R_2 contribute equally to the large internal resistance of 460 MΩ. Upon exposure to hydrogen-in-air mixture, both R_1 and R_2 resistance decreases with increasing time (see Figure 4). Despite the long exposure time of 60 min, the aged sample still shows a large internal resistance ($R_{int} = R_1 + R_2$) of 14.7 kΩ. After flashing, R_1 (176 Ω) becomes six orders of magnitude smaller than the value of R_1 of the aged sample, whereas R_2 (101 kΩ) decreases by three orders of magnitude. The internal resistance of the flashed sample becomes very small and equals 118 Ω at a hydrogen exposure time of 4 min. Furthermore, R_{int} of the flashed sample remains almost constant with increasing t. This is consistent with constant and high values of J_{sc} after flashing.

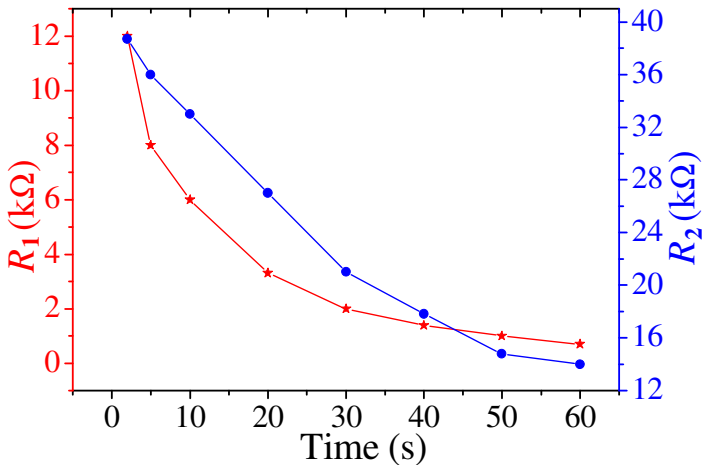

Figure 4. The evolution of grain boundary resistance and charge transfer resistance with hydrogen exposure time.

The large value of the resistance (460 MΩ) of the aged sample is in accordance with the assumption that grain boundaries have a high concentration of oxygen-derived interface states. These states trap, by H_2 adsorption, a major portion of the released electrons and increase the energy barrier to electron transport between adjacent grains. With increasing H_2 exposure times, the observation of the decrease in the resistance of grain boundaries, coinciding with the slow increase

in J_{sc}, indicates that the H_2 molecules gradually reduce the density of oxygen surface acceptor states. But even at t = 60 min, the value of internal resistance is approximately 100 fold larger than that obtained after flashing at a H_2 exposure time of 4 min.

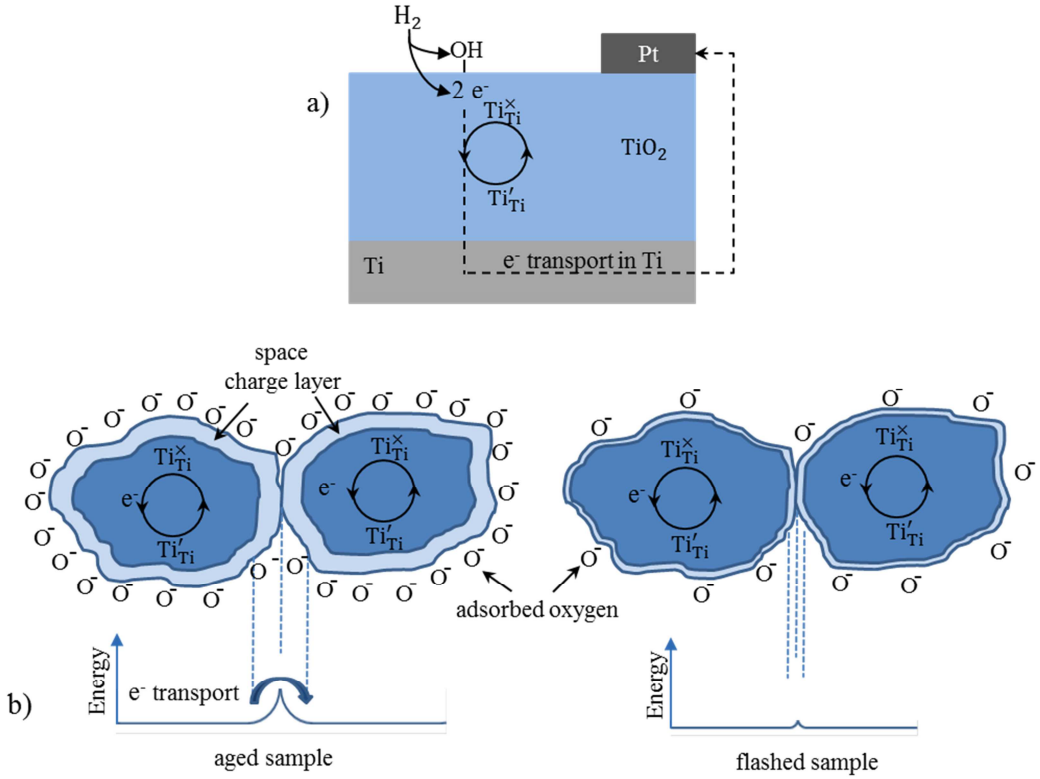

Figure 5 a). Simplified model of surface reactions and charge transfer generating an electrical current. The transport of electrons occurs through the TiO_2 lattice to the titanium contact, from where the electrons flow in the outer circuit to the Pt contact. **b)** Grains of TiO_2 with adsorbed oxygen (only atomic species are shown for simplicity) and formation of the space charge layer for the aged and flashed sample. The density of surface states is significantly reduced by flashing, resulting in a reduction of space charge layer thickness and energy barrier heights between adjacent TiO_2 grains.

In a simplified model of emf generation, Figure 5a depicts selected surface reactions and charge transfers in a porous Pt/TiO_2/Ti structure. For further details of the competed model the reader is referred to the publications [1,5]. The reaction of hydrogen with the lattice oxygen of TiO_2 releases two electrons into the TiO_2 per H_2 molecule, thereby forming the OH surface groups. The electron

transfer occurs through the TiO_2 porous structure via an electron hopping process over Ti^{4+} ions ($Ti_{Ti}^{\times}$ in Kröger-Vink notation) and Ti^{3+} ions (Ti_{Ti}') to the titanium contact. It is evident that oxygen states are removed in ultra-high vacuum, which means that corresponding Ti 2p core level states of Ti_{Ti}' are not seen in XPS (Figure 1d).

We explain that the observed low current densities, even after long H_2 exposure times of the aged samples, originate from a large number of negatively charged acceptor-type oxygen adsorption states at the TiO_2 grains. This in turn leads to space charge layers and, correspondingly, to an energy barrier for electron transport over the boundaries of adjacent TiO_2 crystallites (Fig. 5-bottom left).

Our experiments show a low internal resistance and an almost resistive behavior after flashing of the sample. This observation is consistent with a reduction in the density of surface trap states of oxygen. The concentration of Ti_{Ti}' and hence of mobile electrons is larger than for the aged sample and the energy barrier for electron transport between TiO_2 grains is reduced (Fig. 5-bottom right), which leads to an overall increase in the conductivity of titanium oxide. As a result, the current density of flashed samples in hydrogen-in-air mixtures is drastically improved with respect to aged samples.

3.4 Conclusions

In this work the effect of thermal activation of $Pt/TiO_2/Ti$ emf cells was investigated. We observed that $Pt/TiO_2/Ti$ samples stored in ambient air show a strong aging behavior in terms of emf generation. The aged samples could, after a very short flashing process, be regenerated to their initial active state. The TiO_2 samples were characterized by SEM, AFM, Raman and XPS, and EIS. The SEM and AFM images show that samples have similar porous microstructures before and after flashing. Also, no visible changes in the XPS and Raman spectra of untreated and flashed TiO_2 samples were observed. However, the data from EIS results were found to be consistent with the large differences in the current densities between aged and flashed $Pt/TiO_2/Ti$ samples. We conclude from these

results that aged samples show a significant density of oxygen-derived acceptor-like surface states. Flashing regenerates the aged samples to their initial as-prepared state by reducing the density of adsorbed oxygen.

3.5 References

[1] Schierbaum, K.; El Achhab M. Generation of an electromotive force by hydrogen-to-water oxidation with Pt-coated oxidized titanium foils. *Phys. Status Solidi A* **2011**, .DOI 10.1002/pssa.201127400F.

[2] Karpov, E. G.; Hashemian, M. A.; Dasari, S. K. Chemistry-Driven Signal Transduction in a Mesoporous Pt/TiO_2 System. *J. Phys. Chem. C* **2013**, *117*, 15632-15638.

[3] Hashemian, M. A.; Palacios, E.; Nedrygailov, I. I.; Diesing, D.; Karpov, E. G. Thermal Properties of the Stationary Current in Mesoporous Pt/TiO_2Structures in an Oxyhydrogen Atmosphere. *ACS Appl. Mater. Interfaces* **2013**, *5*, 12375-12379.

[4] Cakabay, Ö.; El Achhab, M.; Schierbaum, K. Thermal properties of solid-state Pt/TiO_2/Ti emf cells studied by microcalorimetry. *Appl. Phys. A* **2015**, *118*, 1127-1132.

[5] Cakabay, Ö.; El Achhab, M.; Schierbaum K. Effect of water vapor on Pt/TiO2/Ti electromotive force cells. *J. Phys. Chem. C* **2016**, DOI: 10.1021/acs.jpcc.6b01315.

[6] Setvin, M.; Aschauer, U.; Scheiber, P.; Li, Y.-F.; Hou, W.; Schmid, M.; Selloni, A.; Diebold, U. Reaction of O_2 with Subsurface Oxygen Vacancies on TiO_2 Anatase (101). *Science 2013*, 341, 988-991.

[7] Li, Y.-F.; Aschauer, U.; Chen, J.; Selloni, A. Adsorption and Reactions of O_2 on Anatase TiO_2. *Acc. Chem. Res.* **2014**, DOI: 10.1021/ar400312t.

[8] Henderson, M. A.; Epling, W. S.; Perkins, C. L.; Peden, C. H. F.; Diebold, U. Interaction of Molecular Oxygen with the Vacuum-Annealed TiO_2(110) Surface: Molecular and Dissociative Channels. *J. Phys. Chem. B* **1999,** *103*, 5328-5337.

[9] Pillay, D.; Wang, Y.; Hwang, G. S. Prediction of Tetraoxygen Formation on Rutile TiO_2(110). *J. Am. Chem. Soc.* **2006**, 128 (43), 14000–14001.

[10] de Lara-Castells, M. P.; Krause, J. L. Theoretical study of the interaction of molecular oxygen with a reduced TiO_2 surface. *Chem. Phys. Lett*. **2002**, 354, 483.

[11] Green, J.; Carter, E.; Murphy, D. M. Interaction of molecular oxygen with oxygen vacancies on reduced TiO_2: Site specific blocking by probe molecules. *Chem. Phys. Lett.* **2009**, 477, 340-344.

[12] Golego, N.; Studenikin, S. A.; Cocivera, M. Effect of oxygen on transient photoconductivity in thin-film $Nb_xTi_{1-x}O_2$, *Phys. Rev. B* **2000**, 61, 8262.

[13] Compton, R. N.; Reinhardt, P. W.; Cooper, C. D. Collisional ionization of Na, K, and Cs by CO_2, COS, and CS_2: Molecular electron affinities *J. Chem. Phys*. **1975**, 63, 3821.

[14] Indrakanti, V. P.; Schobert, H. H.; Kubicki, J. D.Quantum Mechanical Modeling of CO_2 Interactions With Irradiated Stoichiometric and Oxygen-Deficient Anatase TiO_2 Surfaces: Implications for the Photocatalytic Reduction of CO_2. *Energy Fuels* **2009**, 23, 5247-5256.

[15] Indrakanti, V. P.; Kubicki, J. D.; Schobert, H. H. Photoinduced activation of CO_2 on Ti-based heterogeneous catalysts: Current state, chemical physics-based insights and outlook. *Energy Environ. Sci.* **2009**, 2, 745.

[16] Henderson, M. A. Evidence for Bicarbonate Formation on Vacuum Annealed TiO_2(110) Resulting From a Precursor-Mediated Interaction Between CO_2 and H_2O. *Surf. Sci.* **1998**, 400, 203-219.

[17] Thompson, T. L.; Diwald, O.; Yates, J. T. CO_2 as a Probe for Monitoring the Surface Defects on TiO_2(110) Temperature-Programmed Desorption *J. Phys. Chem. B* **2003**, 107, 11700-11704.

[18] He, H.; Zapol, P.; Curtiss, L. A. A Theoretical Study of CO_2 Anions on Anatase (101) Surface. *J. Phys. Chem. C* **2010**, 114, 21474-21481.

[19] El Achhab, M.; Erbe, A.; Koschek, G.; Hamouich, R.; Schierbaum, K. A microstructural study of the structure of plasma electrolytically oxidized titanium foils. *Appl. Phys. A* **2014**, *116*, 2039-2044.

[20] Su, C.; Liu, L.; Zhang, M.; Zhanga, Y.; Shao, C. Fabrication of Ag/TiO_2 nanoheterostructures with visible light photocatalytic function *via* a solvothermal approach. *CrystEngComm.* **2012**, 14, 3989-3999.

Own contribution: 80 %

1. Author

Acknowledgments

First of all, I would like to express my deepest gratitude to Prof. Dr. Klaus Schierbaum for the friendly reception in their work group for the constant support, helpful discussions and suggestions.

Moreover, I would like to thank Prof. Dr. Mathias Getzlaff for secondary appraisal of my thesis as well as to Dr. Ulrich Hagemann for the cooperation in carrying out different spectroscopic measurements (SEM, XPS, AFM and Raman).

Special thanks to Dr. Erdal C. Oğuz for proofreading.

My thanks go also to my friends and colleagues in the Materials Science Department for the friendly working atmosphere, discussions and support.

Finally, I am grateful to my family for all their support and patience.

Erklärung

Ich versichere an Eides Statt, dass die Dissertation von mir selbständig und ohne unzulässige fremde Hilfe unter Beachtung der „Grundsätze zur Sicherung guter wissenschaftlicher Praxis an der Heinrich-Heine Universität Düsseldorf“ erstellt worden ist.

Düsseldorf, den 20.07. 2016

……

Ömer Cakabay